Journal Pre-proofs


Full-length Article

# Subacute cytokine changes after a traumatic brain injury predict chronic brain microstructural alterations on advanced diffusion imaging in the male rat

Xuan Vinh To, Abdalla Z. Mohamed, Paul Cumming, Fatima A. Nasrallah

PII: S0889-1591(22)00046-0
DOI: https://doi.org/10.1016/j.bbi.2022.02.017
Reference: YBRBI 4793

To appear in: *Brain, Behavior, and Immunity*

Received Date: 27 September 2021
Revised Date: 7 February 2022
Accepted Date: 12 February 2022

Please cite this article as: Vinh To, X., Mohamed, A.Z., Cumming, P., Nasrallah, F.A., Subacute cytokine changes after a traumatic brain injury predict chronic brain microstructural alterations on advanced diffusion imaging in the male rat, *Brain, Behavior, and Immunity* (2022), doi: https://doi.org/10.1016/j.bbi.2022.02.017

# Subacute cytokine changes after a traumatic brain injury predict chronic brain microstructural alterations on advanced diffusion imaging in the male rat

Xuan Vinh To[1], Abdalla Z Mohamed[1,2], Paul Cumming[3,4], and Fatima A. Nasrallah*[1,5]

[1]*The Queensland Brain Institute, The University of Queensland, Queensland Australia*

[2]*Thompson Institute, University of the Sunshine Coast, Queensland, Australia.*

[3]*Department of Nuclear Medicine, Bern University Hospital, Bern, Switzerland*

[4]*School of Psychology and Counselling, Queensland University of Technology, Brisbane, Queensland, Australia*

[5]*The Centre for Advanced Imaging, The University of Queensland, Queensland Australia*

*Corresponding author

Fatima A. Nasrallah

The Queensland Brain Institute, The University of Queensland

Building 79, Upland Road, Saint Lucia, Brisbane, Queensland, Australia 4072

Phone: +61 7 33460322

Fax +61 7 3346 6301

Email: f.nasrallah@uq.edu.au

## Highlights

- Plasma levels of IL-1$\beta$, IL-7, CCL3, and GM-CSF were elevated from days 3 to 60 post-injury.
- Day 7 plasma marker panels were associated with trans-hemispheric cortical map transfer outcome.
- High IL-1$\beta$ and low IL-7, CCL3, and GM-CSF plasma levels at day 60 associated with worse pathology.

## Abstract

***Introduction:*** The process of neuroinflammation occurring after traumatic brain injury (TBI) has received significant attention as a potential prognostic indicator and interventional target to improve patients' outcomes. Indeed, many of the secondary consequences of TBI have been attributed to neuroinflammation and peripheral inflammatory changes. However, inflammatory biomarkers in blood have not yet emerged as a clinical tool for diagnosis of TBI and predicting outcome. The controlled cortical impact model of TBI in the rodent gives reliable readouts of the dynamics of post-TBI neuroinflammation. We now extend this model to include a panel of plasma cytokine biomarkers measured at different time points post-injury, to test the hypothesis that these markers can predict brain microstructural outcome as quantified by advanced diffusion-weighted magnetic resonance imaging (MRI).

***Methods*:** Fourteen 8–10-week-old male rats were randomly assigned to sham surgery (n = 6) and TBI (n = 8) treatment with a single moderate-severe controlled cortical impact. We collected blood samples for cytokine analysis at days 1, 3, 7, and 60 post-surgery, and carried out standard structural and advanced diffusion-weighted MRI at day 60. We then utilized principal component regression to build an equation predicting different aspects of microstructural changes from the plasma inflammatory marker concentrations measured at different time points.

***Results*:** The TBI group had elevated plasma levels of IL-1$\beta$ and several neuroprotective cytokines and chemokines (IL-7, CCL3, and GM-CSF) compared to the sham group from days 3 to 60 post-injury. The plasma marker panels obtained at day 7 were significantly associated with the outcome at day 60 of the trans-hemispheric cortical map transfer process that is a frequent finding in unilateral TBI models.

***Discussion:*** These results confirm and extend prior studies showing that day 7 post-injury is a critical temporal window for the reorganisation process following TBI. High plasma level of IL-1$\beta$ and low plasma levels of the neuroprotective IL-7, CCL3, and GM-CSF of TBI animals at day 60 were associated with greater TBI pathology.


***Keywords:*** Traumatic brain injury; controlled cortical impact; diffusion-weighted; magnetic resonance imaging; neuroinflammation; cytokines; plasma markers; trans-hemispheric cortical map transfer.

## 1 Introduction

Traumatic brain injury (TBI) is a leading cause of mortality and morbidity globally, with an estimated global prevalence of 295 per 100,000 population.[1] TBI is defined as "an alteration in brain function, or other evidence of brain pathology, cause by an external force".[2] The severity of acute TBI is traditionally classified using the Glasgow Coma Scale,[3] but there is an increasing appreciation of the complex and diverse nature of TBI and its long term sequelae, which include neuronal cell loss, axonal damage, demyelination, and neuroinflammation.[4–7] As such, it is very difficult to make accurate prognosis based purely on clinical symptoms around the time of injury.[8] However, neuroinflammation is now receiving significant attention as potential prognostic indicator of long term outcome, while also presenting a promising interventional targets to improve patients' outcomes in the aftermath of a TBI.[8]

Following TBI, cellular mediators of neuroinflammation release several biomarkers, which make their way into the cerebrospinal fluid or blood, where their concentration may have diagnostic and prognostic potential.[9,10] Notably, plasma and cerebrospinal fluid (CSF) tumour necrosis factor alpha (TNF-$\alpha$) and various interleukins (IL-1$\beta$, IL-6, IL-8, and IL-10) have been suggested as markers for classification and outcome prediction following a TBI.[11] Other plasma biomarkers derived from injured neurons, microglia, and astrocytes have also be considered for this purpose, notably S100 astroglial calcium-binding protein beta (S100β), glial fibrillary acidic protein (GFAP), neuronal specific enolase (NSE), and ubiquitin C-terminal hydrolase-L1 (UCH-L1).[12–15] Nevertheless, early studies on the role of inflammatory biomarkers for predicting TBI outcome often suffered from a reductionist approach focusing on tracking the evolution of a single marker over time, and from oversimplification of the complex cytokine/chemokine interactions. Furthermore, in a clinical setting, TBI pathobiology and outcome can be exacerbated and modified through systemic inflammation due to concomitant peripheral injury.[16] The prognostic value of peripheral inflammatory markers is

thus influenced by the polytrauma typical of real-world human TBI cases, although advance bioinformatics methods can potentially distinguish between peripheral inflammatory characteristic of TBI versus those due to polytrauma.[17] The effects of head injury on blood-brain barrier[18] and glymphatic system function [19] also contribute to the difficulty in developing reliable blood-based biomarkers of TBI.[20]

Given the complexity of human TBI and its potential for interaction with a systemic immune response, an animal model of TBI such as the controlled cortical impact (CCI) model in rats[21] provides a robust platform for translational research with minimized individual variability, while capturing many of the ongoing pathologies typically seen in human TBI survivors.[22] Furthermore, a rat TBI model combined with a panel of cytokine expression in brain[23] or PCR microarray analysis of mRNA expression in spleen or thymus[24] can give extra dimensions to the study of inflammatory changes in the injured brain. Structural magnetic resonance imaging (MRI) and diffusion tensor imaging (DTI) are commonly used to monitor brain anatomic and microstructural alterations in human TBI[25–27] and experimental animal TBI.[6,28–30] DTI gives an index of fractional anisotropy (FA), which is generally reduced in conjunction with traumatic white matter and axonal injury.[6,31] While DTI is the de facto standard clinical diffusion MRI, its specificity is imperfect.[32] For example, FA reduction might be caused by reduced density of neurite (axons and dendrites), increased dispersion in neurite orientation, or their demyelination, among other possible changes.[33] Neurite orientation dispersion and density imaging (NODDI) is an advanced diffusion MRI modality approach designed to provide greater specificity to diffusion MRI changes.[34] NODDI purports to separate the water diffusion signal into non-exchanging compartments: the isotropic free water (i.e., CSF), intra-neurite (i.e., axons and dendrites), and extra-neurite (i.e., extracellular water, neuronal cell bodies and glial cells) fractions, potentially better reflecting the true complexity of brain tissue microstructural.[34] A number of histological validation studies on animal models

have contrasted NODDI metric change fingerprints versus biophysical changes. For example, ex vivo NODDI imaging of a mouse cuprizone model of demyelination showed decreased Neurite Density Index (NDI) without concomitant Orientation Dispersion Index (ODI) changes.[35] We hypothesised that early post-TBI plasma inflammatory marker panels should predict the long-term/chronic microstructural outcomes measured with NODDI in the rodent TBI model.

## 2 Materials and Methods

### *2.1 Experimental design*

The study was approved by the Animal Research Ethics Committee (AEC) of the University of Queensland (IRB number: QBI/036/16/MAIC). Fourteen Sprague-Dawley male rats (8–10 weeks old, 300–340 g) were purchased from the Animal Resource Centre (ARC, Western Australia) and housed under conventional laboratory conditions with a 12-hour light-dark cycle and ad libitum access to food and water. Rats were randomly assigned to one of two groups: sham surgery (n = 6) and TBI (n = 8). Blood samples were drawn from the tail vein and the plasma fractions were separated and frozen for later analysis at days 1, 3, 7, and 60, whereas MRI scans were conducted at day 60 after surgery. Plasma marker panels of cytokines were conducted to provide immunological biomarker fingerprints at day 1, 3, 7, and 60 post-TBI.

Experimenters were not blinded to the animal's experimental conditions, but personnel conducting the data processing and analysis were blinded (although TBI animals usually had obvious and gross structural changes visible on structural MRIs), and all MRI data were processed semi-automatically through a processing pipeline. While there is a growing debate on the effects of sex differences in TBI outcome,[36] we decided to use male rats to reduce one potential confounding factor and maintain consistency with our earlier studies.[29,30]

### *2.2 Controlled cortical impact (CCI) traumatic brain injury model*

The CCI procedure was outlined in our previous publication.[30] In brief, rats were anaesthetized with isoflurane (5% for induction, 1–2% for maintenance) in a 40:60 $O_2$:medical air gas mixture delivered a flow rate of 2 L/min. The rats were transferred to a stereotaxic frame and a 5 mm diameter craniotomy window was created over the right hemisphere centred at 2.5 mm posterior to Bregma and 3 mm right lateral to the sagittal suture, taking care not to damage the underlying dura. The bone flap was removed to expose the dura matter, and a CCI injury was delivered to animals in the TBI group using a pneumatically driven impactor (TBI 0310, Precision System and Instrumentation, USA) with a cylindrical 4 mm diameter tip. Impact parameters were as followed: impact velocity = 5 m/s, penetration depth = 2 mm, and dwell time = 200 ms. For sham animals, craniotomy was performed as above, but no actual impact was delivered. After the impact or sham procedure was completed, the bone flap was replaced over the craniotomy window and the scalped sutured. Total time under anaesthesia was less than 20 minutes. Animals was removed from the stereotaxic frame and placed on a heated surface for monitoring and recovery. Animals were returned to their home cage after they had recovered and appeared fully mobile and alert. Overall, no animals showed conspicuous signs of motor deficits after the procedure.

### *2.3 Blood sample collection and inflammatory marker quantification*

Blood sample collection at each timepoint (days 1, 2, 7, and 60 post-procedure) was performed by tail vein venepuncture and blood collection into a 1.5 ml Eppendorf tube coated with 8 $\mu$L of 0.5 M EDTA. An additional volume of EDTA solution was added to blood samples to reach a final 5 mM concentration. Blood samples were centrifuged at 3,000 rpm at 4 ℃ for 15 minutes, and the plasma was then filtered through glass wool by re-centrifugation at 3,000 rpm at 4 ℃ for 15 seconds, and then passed through a 0.22-micron filtration column by

centrifugation at 5,000 rpm at 4 ℃ for 60 seconds. The filtered plasma samples were stored at -80 ℃ for further analysis.

Immunological marker analysis was performed using the rat cytokine kit from Bio-Rad (Cat# 12005641). Plasma samples were thawed and diluted as per the manufacturer's instruction by mixing one volume of plasma and three volumes of the sample diluent provided in the kit. Diluted plasma samples were centrifuged at 14,000 g for five minutes to sediment any remaining cells, and the supernatants were analysed for content of 23 markers: granulocyte colony-stimulating factor (G-CSF), granulocyte-macrophage colony-stimulating factor (GM-CSF), macrophage colony-stimulating factor (M-CSF), growth-regulated oncogene/keratinocyte chemoattractant (GRO-KC), interferon gamma (IFN-$\gamma$), monocyte chemoattractant protein-1 (MCP-1), the interleukin IL-1$\alpha$, IL-1$\beta$, IL-2, IL-4, IL-5, IL-6, IL-7, IL-10), IL-12p70, IL-13, IL-17$\alpha$, IL-18), and the chemokine (C-C motif) ligands CCL3, CCL5), and CCL20, as well as tumour necrosis factor alpha (TNF-$\alpha$), and vascular endothelial growth factor (VEGF). Analytes were detected simultaneously in 96-wells plates. Standards and samples were assayed on the robotic liquid handling workstation epMotion 5075 (Eppendorf), the assay plates were washed on the Bio-Plex Pro II magnetic plate washer (Bio-Rad), and the plates were read with the Bio-Plex Systems 200 (Bio-Rad). As per the instructions, 50 µl portions of 1:3 diluted plasma per well were incubated at room temperature in the dark with antibody-coupled magnetic beads for 60 min. After washing, the beads were incubated with the detection antibody for 30 min. The antibody conjugates were then incubated with Streptavidin for 10 min, washed, resuspended and vortexed prior to reading on the Bio-Plex system. Samples analysis and standard curves [Log(x) - Linear(y)] were generated using the Bio-Plex Manager v6.1 software (Bio-Rad).

### *2.4 Magnetic Resonance Imaging (MRI) procedure*

#### *2.4.1 Animal handling*

Anaesthesia for MRI scans was induced with isoflurane (4% induction, 1–2% during preparation, and 0–0.3% during scanning) in 40:60 $O_2$ : medical air gas mixture delivered at a flow rate of 2L/min in an anaesthesia box. An intraperitoneal (IP) catheter was inserted and fixed in place for delivery of medetomidine (Domitor, Pfizer, Germany). Each rat was positioned on an MRI-compatible cradle (Bruker Biospin, Germany) with ear bars and bite bars to reduce head motion. A rectal thermometer was inserted, and monitoring of respiration rates and patterns, and rectal temperature was achieved using a MR-compatible monitoring and gating system for small animals (Model 1030, Small Animal Instruments, New York, the USA). After positioning of the animal within the bore of the MRI scanner, medetomidine (0.1 mg/kg) was administered as a bolus followed immediately by the start of a continuous infusion (0.1 mg/kg/h). The respiration rate was in the range of 60–95 breaths per minute. The animal's body temperature was maintained at 36 ± 1 ℃ by warm water circulating in tubes embedded in the animal holding cradle (SC100, Thermo Scientific, USA). At the end of the scan, 0.1 mg/kg atipemazole was administered as an intraperitoneal bolus for medetomidine reversal (Antisedan, Pfizer, Germany).

#### *2.4.2 MRI scans*

As described in our previous publications,[29,30] MRI scans were acquired using 9.4 T Bruker system (BioSpec 94/30USR, Bruker, Germany) and the software Paravision 6.0.1 (Bruker, Germany), along with a volume transmitter coil and a four-element array receiver coil. Anatomical imaging was performed using T2-weighted rapid-relaxation-with-enhancement (RARE) sequence with the following parameters: repetition time (TR)/Echo Time (TE) = 5900/65 ms, RARE factors = 8, number of averages = 2, FOV = 25.6 × 32 mm, matrix size =

256 × 256 × 40, and 0.5 mm-thick slices, giving an effective output spatial resolution of 0.1 × 0.125 × 0.5 mm. Diffusion-weighted images were collected using a spin-echo echo-planar imaging (EPI) sequence with TR/TE = 10000/29 ms, FOV = 24.8 × 24.8 mm, matrix size = 108 × 108 × 41, and 0.5 mm-thick slices with 0.1 mm slice gaps, giving effective output spatial resolution of 0.23 × 0.23 × 0.6 mm. Two b-value shells of 750, 1500 s/mm$^2$, with 32 diffusion-weighted directions per shell, and 4 volumes of b = 0 s/mm$^2$ were acquired.

### *2.5 MRI data processing*

Data from the MR scanner were exported to DICOM format using Paravision 6.0.1 and converted to NIFTI data format using MRIcron.[37] Structural images were given a header file with voxel size ten times larger than the original voxel size as an adaptation to image processing tools originally developed for human brain.[3] Structural image pre-processing was performed as follows: signal inhomogeneity correction was performed on T2-weighted structural images using N4ITK bias field correction[38] as implemented in the Advanced Normalisation Tool (ANTs v.2.3.4).[39] Brain-masking or skull-stripping was performed on signal inhomogeneity-corrected images using 3D pulse-coupled neural networks (PCNN)[40] following by manual editing. For animals in the TBI group, we manually adjusted brain masks to exclude the lesion area, defined as areas with obvious hyper- or hypo-intensity and/or tissue loss. The pre-processed and masked structural images of the sham animals were linearly registered to the masked SIGMA *in vivo* rat brain template,[41] using the FSL (v.6.0.4 https://fsl.fmrib.ox.ac.uk/fsl/fslwiki) program FLIRT.[9] The sham group's linearly registered structural images were then used for an iterative non-linear image registration/template construction procedure using the Advanced Normalization Tool (ANTS v.2.3.4[42] MultivarateTemplateConstruction2.sh) to create a study-specific sham structural template. Spatial normalisation of structural images of sham and TBI animals (TBI animals' images have

visible focal lesions) to the template was accomplished using the constrained cost function masking (CCFM) approach, which is an extension of the original cost function masking approach.[43] We implemented the CCFM approach by registering the study-specific sham template to each animals' pre-processed and masked structural images with an additional cost function mask that included only the "normal" parts of the brain and exclude the lesion area, using Symmetric Diffeomorphic Image Registration with Cross-Correlation (SyN-CC),[44] as implemented in ANTS. The resulting subject-specific transformation was inversed to allow for warping of each subject's structural image to the study-specific sham template and a common space. The image registration process also generated the Jacobian Index (JI) maps, which are 3D images that indicate the relative volume change required to warp the template voxel to the individual voxel.

The four b = 0 volumes were averaged to generate the b = 0 spatial representation of diffusion MRI data. Diffusion MRI data were corrected for motion and eddy current using FSL's *eddy_correct* with the spatial representation of diffusion MRI data serving as the reference. The b = 0 spatial representation image was corrected for signal inhomogeneity using the N4ITK bias field correction[38] as implemented in ANTs (v.2.3.4).[39] A special brain mask in diffusion MRI space was generated for each rat by affine registration of the inhomogeneity-corrected b = 0 diffusion MRI spatial representation (with the ten-fold enlarged header file) to the signal inhomogeneity-corrected T2-weighted structural images, and the inverted transformation was then used to resample the structural brain mask (lesion-included) to the diffusion MRI space. Diffusion MRI data were fitted using Neurite Orientation Dispersion and Density Imaging (NODDI) using the NODDI MATLAB toolbox (https://www.nitrc.org/projects/noddi_toolbox).[34,45] Intra-neurite diffusion in each voxel was modelled as diffusion in zero radius cylinders, with the assumption of no lateral diffusion occurring between the neurites and a homogenous cell background; the neurite "cylinders'"

orientation was modelled as Watson's distribution and the NODDI algorithm used Szafer et al.'s tortuosity model for randomly packed cylinders.[46] Fixed intrinsic diffusivity and fixed isotropic diffusivity were assumed to be $1.4 \times 10^{-9}$ $m^2/s$ and $4 \times 10^{-9}$ $m^2/s$, respectively. The following NODDI metric images were obtained as readouts: neurite density index (NDI), orientation dispersion index (ODI), and isotropic diffusion volume fraction (fISO).

Each rat's signal inhomogeneity-corrected and masked spatial representation of the diffusion MRI image was registered to the corresponding rat's pre-processed and masked (lesion-included) structural image using the ANTS SyN-CC registration. The warping field obtained from this step was combined with the individual structural image to template warping fields to warp the NODDI metric images (NDI, ODI, and fISO) to the study-specific sham template.

Diffusion tractography was employed to map structural connectivity in this study using the global tractography approach,[47,48] which leveraged the multi-shell diffusion data and was implemented as *tckglobal* in MRtrix3® (https://www.mrtrix.org/).[49] Tissue response function was estimated using the Dhollander algorithm,[50,51] implemented as *dwi2response dhollander* in MRtrix3®. In global tractography, connectivity streamlines are built from segments called particles (particle length was set to 0.1 mm for our data), particle potential was set to 0.01 and connection potential set to 5. Whole brain parcellation map in the SIGMA *in vivo* rat brain template was warped into each individual rat's diffusion-weighted data space using the inverse warping fields of the image registration process described and the parcellation map in subject's space was used as nodes for whole-brain structural connectivity calculation. Structural connectivity matrix was calculated based on the streamline tractography using MRtrix3®'s *tck2connectome*, with the connectivity metric scaled as the number of streamlines connecting the two nodes; each streamline was assigned to all nodes that it intersected along its length (-assignment_all_voxels option).

### *2.6 Statistical analysis*

#### *2.6.1 Group comparisons of inflammatory biomarkers*

Unpaired Mann-Whitney tests comparing the levels of plasma inflammatory biomarkers were performed to compare sham and TBI groups at different timepoints; multiple comparison corrections were performed using false discovery rate (FDR) and a threshold was set at the desired FDR (Q) < 0.1. Statistical analysis was performed in Prism 9 (GraphPad Inc., CA, USA).

#### *2.6.2 Regression analysis of diffusion MRI outcomes at day 60 post-injury and TBI animals' inflammatory marker panels.*

Data reduction for TBI group's plasma cytokine markers at each timepoint was performed using principal component analysis (PCA) using Prism 9. In brief, the plasma concentrations of each marker across all TBI animals at each timepoint were standardised and centred so that the mean of each marker was zero and the standard deviation was one. Separate PCAs were performed for the rats' centred and standardised inflammatory marker levels at each time point. The number of principle components (PCs) was chosen so that the PCs cumulatively explained at least 90% of the variance in the inflammatory marker panels at each timepoint, and a maximum of four PCs were extracted for subsequent regression analysis to minimise over-fitting.

The extracted principal components values were used to perform voxel-wise multiple linear regression predicting NODDI metrics outcomes at 60 days post-injury using each TBI rat's plasma inflammatory marker panel at each time point. Voxel-wise multiple linear regression analysis was performed by permutation inference for the general linear model[52] as implemented in FSL's *randomise*,[53] with the number of permutations set to 10,000 or exhaustive, whichever was smaller. The resulting statistical maps were corrected for multiple

comparisons with mass-based FSL's threshold-free cluster enhancement (TFCE)[54] and a threshold was set at P value < 0.05 (two-tailed).

The voxel-wise regression analysis identified several NODDI metrics-of-interests in specific regions-of-interest (ROIs) in the brain of injured animals that could be predicted by the animals' plasma cytokine panels. The NODDI metrics-of-interest values of TBI animals were extracted from these ROIs, namely the NDI in the ipsilateral and contralateral (to the injury) cortex and the fISO in the ventricles. The voxel-wise regression analysis identified that the NODDI metrics-of-interest were found to be correlating with the animals' plasma cytokine panels in the ipsilateral and contralateral (to the injured cortex) lateral parietal associative cortices (LPACs). The total number of streamlines connecting these each of these parcellations to the rest of the brain were quantified. Statistical map results of voxel-wise regression analysis and the ROIs of the NODDI metrics-of-interest are presented in Supplementary Figure 1. Principal component regression (PCR) was performed using Prism 9 (GraphPad Inc., CA, USA) to predict the NODDI metrics-of-interests in the ROIs and the total number of streamlines connecting each of the ipsilateral and contralateral LPAC to the rest of the brain from the plasma inflammatory panels of TBI animals at each timepoint. The numbers of PCs were chosen to cumulatively explain at least 90% of the variances in the inflammatory panels at each timepoint, with extraction of a maximum of four PCs to avoid over-fitting.

#### *2.6.3 Group comparisons of diffusion MRI metrics and tensor-based morphometry*

Group comparisons of spatially normalised DTI, FA, NODDI metrics (NDI, ODI, and fISO), and JI (tensor-based morphometry[55]) were performed using permutation inference for the general linear model[52] as implemented in FSL's *randomise*,[53] with the number of permutation set to 10,000 or exhaustive, whichever was smaller. The resulting statistical maps were corrected for multiple comparisons with the FSL mass-based threshold-free cluster

enhancement (TFCE)[54] and a threshold was set at P value < 0.05 (two-tailed).

Repeated measures two-way Analysis of Variance (ANOVA) was performed to analyse the effect of traumatic brain injury and the ipsi- versus contra-lateral effects on the number of diffusion tractography streamlines from the LPAC. Post-hoc Fisher's least significant difference test was used to perform post-hoc statistical tests.

Correlation analyses were performed between the NDI quantified from the ipsi- and contra-lateral cortical areas, the NDI from the contralateral cortical area and the number of tractography streamlines connected to the contralateral LPAC, and the number of streamlines connected to the ipsi- and contra-lateral LPAC.

## 3 Results

### *3.1 Longitudinal changes in plasma inflammatory markers in a rat CCI model of TBI*

The TBI animals showed significantly lower plasma levels of IL-12p70, IL-1$\alpha$, and M-CSF at day 1 after the injury (Figure 1). The levels of these three markers normalised relative to the sham groups at times after day 1. There were elevated plasma levels of IL-1$\beta$, IL-7, GM-CSF and CCL3 in the TBI-injured animals at days 3, 7, and 60 post-injury (Figure 1). The remaining markers did not show significant differences between the TBI and sham groups; nevertheless, in a subset of 3 TBI subjects, IL-2, IL-4, IL-5, IL-6, IL-13, IL-17$\alpha$, IL-19, G-CSF, and IFN-$\gamma$ levels were consistently elevated between day 1 and day 7 compared to all other sham and TBI animals (Figure 2); these animals are called "very high cytokine TBI" and despite the consistently elevated plasma cytokine levels, they did not have distinctive brain injury or lesion characteristic compared to other TBI animals. Examples of structural images, NODDI metric images, and diffusion tractography of sham, very high cytokine TBI, and other TBI animals are shown in Figure 3.

The levels of other markers that showed unremarkable differences are shown in Supplementary Figure 1.

### *3.2 Correlation of longitudinal inflammatory levels with microstructural outcomes*

Principal component regression analysis (PCRA) showed that day 7 cytokine panel results predicted NDI values at day 60 after TBI in the ipsi- and contralateral cortex, whereas fISO values in the lateral ventricles were associated with day 60 cytokine panel results. Specifically, the centred and standardised NDI values in the contralateral cortex were predictable from day 7 centred and standardised plasma IL-6, G-CSF, IFN-γ, IL-19, IL-12p70, IL-13, IL-17α, IL-18, IL-1α, IL-2, IL-4, IL-5, M-CSF, and TNF-α (positive estimates), and GRO/KC, MCP-1, CCL3, CCL5, and VEGF (negative estimates). The regression equation was significant (F [4, 3] = 53.9, P value = 0.004), with an $R^2$ of 0.986 (Table 1), thus accounting cumulatively for almost all of the variance in NDI. Centred and standardised NDI values in the ipsilateral cortex at day 60 could be predicted using centred and standardised plasma GRO/KC, IL-1β, MCP-1, GM-CSF, CCL3, CCL5, VEGF (positive estimates), and G-CSF, IL-12p70, IL-13, M-CSF, and TNF-α (negative estimates) levels at day 7 post-injury. The regression equation was significant (F [4, 3] = 28.5, P value = 0.01), with an $R^2$ of 0.974 (Table 2). Centred and standardised fISO values in the ventricles of TBI animals at day 60 post-injury could be predicted from day 7 centred and standardised plasma levels of IL-6, G-CSF, IFN-γ, IL-13, IL-17α, IL-18, IL-1β, IL-2, IL-4, TNF-α (positive estimates), and GRO/KC, IL-19, IL-12p70, IL-1α, IL-5, M-CSF, MCP-1, GM-CSF, CCL3, CCL20, CCL5, and VEGF (negative estimates). The regression equation was significant (F [4, 3] = 639, P value = 0.0001), with an $R^2$ of 0.999 (Table 3). Centred and standardised number of tractography-identified streamlines through the contralateral LPAC in TBI animals at day 60 post-injury could be predicted from day 60 centred and standardised plasma levels of IL-19, IL-12p70, IL-17α, IL-1α, IL-5, M-CSF,

CCL20, CCL5 (positive estimates), and IL-6, G-CSF, GRO/KC, IFN-γ, IL-1β, IL-7, GM-CSF, TNF-α (negative estimates). The regression equation was significant (F [4, 3] = 27.7, P value = 0.0105) with an $R^2$ of 0.974 (Table 4).

### *3.3 Group difference in NODDI metrics at day 60 post-procedure*

Group comparisons of spatially normalised NODDI metrics showed that TBI animals had decreased ODI in the bilateral caudate-putamen and ipsilateral hippocampus to the lesion, decreased NDI in the bilateral anterior external capsule and ipsilateral cortical area, and increased fISO in the ventricles and the impacted cortical area (Figure 4).

Repeated measures two-way ANOVA (Table 5 and Figure 5a) revealed significant interaction between the effects of TBI and ipsi- versus contra-lateral on the number of streamlines connected to the LPAC (F [1, 12] = 7.088, P value = 0.0207). Simple main effects analysis showed TBI animals had significantly fewer tractography streamlines to the LPAC at day 60 post-injury (Table 5 and Figure 5, F [1, 12] = 5.601, P value = 0.0356, 95% Confidence Interval [CI] of difference = 3.87 – 93.71). The analysis did not find significant main effect for ipsi- versus contra-lateral cortex on the number of streamlines connected to the LPAC (Table 5, F [1, 12] = 0.000292, P value = 0.987, 95% CI of difference = -26.36 – 26.77). Post-hoc test revealed that there was significantly fewer tractography streamlines connected to the ipsilateral LPAC in the TBI group than the sham group (sham – TBI, ipsilateral: P value = 0.0024, 95% CI of difference = 31.82 – 130.7. Table 5). In the TBI group, the difference in the number of tractography streamlines connected to the ipsilateral compared to the contralateral LPAC approached statistical significance (ipsilateral – contralateral, TBI: P value = 0.1017, 95% CI of difference = -7.49 – 72.83. Table 5).

There was significant correlation between the NDI quantified from the ipsi- and contra-lateral cortical area ROIs (Figure 5b, Pearson r = -0.656, P value = 0.039, one-tailed). There

was insignificant correlation between the NDI quantified from the ipsilateral cortical ROI and the number of streamlines connected to the contralateral LPAC (Figure 5c, Pearson r = 0.178, P value = 0.336, one-tailed) or between the number of streamlines connected to the ipsi- and contra-lateral LPAC (Figure 5d, Pearson r = 0.24, P value = 0.283, one-tailed).

## 4 Discussion

We found that acute/subacute peripheral plasma inflammatory marker panel results at day 7 after the injury served as powerful predictors of chronic/long-term brain microstructural outcomes as detected by diffusion MRI in a rat CCI model of moderate-severe open-head TBI. The panel's prognosis efficiency varied temporally for different aspects of the injury-recovery process. Specifically, advanced diffusion MRI detected signs consistent with the cortical reorganisation and trans-hemispherical transfer at day 60 post-injury. Day 7, but not day 1 or 3 post-injury neuroinflammatory marker panel results predicted the subsequently declining neurite density in the ipsilateral cortex and gain in the contralateral cortex; we think this reflected the short-range connectivity changes in the cortex. Thus, day 7 blood chemistry findings propagated to late changes in the organization of cerebral cortex. On the other hand, the day 60 neuroinflammatory marker panel results while not correlating with neurite density in the cortical regions, they were correlating with the number of diffusion tractography streamlines connecting the contralateral cortex to the rest of the brain at day 60 post-injury; we think this reflected longer range connectivity changes. The day 60 neuroinflammatory marker panel also correlated with the degree of isotropic diffusion fraction in the ventricles at day 60 post-injury; isotropic diffusion in the ventricle straightforwardly reflected the degree of hydrocephalic pathology. A summary of the imaging findings and their relationship with the plasma markers is presented in Figure 6.

### *4.1 Temporal dynamics of inflammatory markers following injury*

We saw an initial decline of plasma levels of classical inflammatory cytokines such as IL-1$\alpha$ at day 1 post-injury. This might seem counterintuitive, given the expectation of an acute inflammatory progression post-TBI, and given earlier results showing that brain levels of IL-1$\alpha$ and IL-1$\beta$ levels rapidly increased post-TBI in a similar rat models of TBI.[56–59] However, it is notable that quantification of IL-1$\alpha$ and IL-1$\beta$ brain levels was generally performed earlier than 24 hours post-injury in prior rodent studies.[58–60] In the drop weight model of TBI, brain levels of IL-1$\beta$ increased within the first hour, peaked at 16 hours, and had mostly normalised at 24 hours post-injury, whereas IL-1$\beta$ was not elevated in the plasma or liver over the same interval.[60] In the present study, the plasma IL-1$\alpha$ level was initially lower in TBI animals than in the sham group and then normalized, whereas the plasma IL-1$\beta$ level was persistently elevated from day 3 onwards. In a sterile model of hypoxia-induced neuroinflammation, IL-1$\alpha$ was released from dying cells earlier than IL-1$\beta$ and had a functional role in neutrophil recruitment to brain, while IL-1$\beta$ was released later and seemed responsible for the propagation of inflammation and recruitment of macrophages.[61] Thus, the acute phase of inflammation in the post-hypoxic brain was resolved on day 1 post-injury, and brain inflammatory cytokines may not have perturbed the levels in systemic circulation. In the context of Alzheimer's disease, peripheral inflammatory markers are only modestly associated with markers of disease pathology and neuronal damage.[62] Thus, there need be no strong relationship between chronic neuropathology with plasma marker levels.

We also found persistently elevated plasma levels of IL-1$\beta$, IL-7, and CCL3 from day 3 until day 60 post-injury, whereas the GM-CSF concentration was elevated from day 3 to day 7 post-injury. Elevated levels of IL-1$\beta$ were found in the serum of humans with moderate-severe TBI within 24 hours[63] and up to a week post-injury.[64] We suppose that the acute phase of TBI-induced neuroinflammation was resolved in the present model on day 1 post-injury, as

likewise reported for brain IL-1$\beta$ levels in another rat TBI study.[60] Nonetheless, IL-1$\beta$ may also have a role in ongoing immune activation and/or immune-system-modulation of injured brain tissue. Since IL-1$\beta$ is produced in brain by activated macrophages and microglia,[65] and considering that the CCI model provokes chronic activation of microglia,[66] present findings of elevated plasma IL-1$\beta$ may be an indicator of chronic neuroinflammation in the post-TBI brain. Inducing a systemic inflammation by administration of IL-1$\beta$[67] or lipopolysaccharide[68] can exacerbate neuroinflammation and worsen the outcome in rodent TBI models. IL-7 is also known as an anti-inflammatory/neuroprotective cytokine and CCL3 is an anti-inflammatory chemokine, both of which show upregulated mRNA expression in peripheral blood from rats with lateral fluid percussion brain injury.[69] GM-CSF is another cytokine with a neuroprotective function post-TBI, as revealed through interventional studies involving GM-CSF.[70–72] In a human stem cell model of the inflammatory response post-TBI, IL-7 and GM-CSF were induced by the addition to the incubation medium of IL-6 and TNF-α.[73] While the plasma concentrations of neither IL-6 nor TNF-α were elevated in this study post-injury, IL-6, which is expressed by resident glial and neuronal cells,[74] shows increased expression in the brain of the rat CCI model of TBI at day 6 post-injury,[75] and TNF-α is released from microglia and astrocytes shortly after TBI. Thus, it is plausible that the present anti-inflammatory responses were induced by the early (< 24 hours post-injury) inflammatory cytokine response in the central nervous system (that resolved within 24 hours). Contrary to the known rapid resolution of central inflammatory responses, the anti-inflammatory responses were systemic and sustained.

### *4.2 Microstructural alterations following injury revealed by MRI*

Our advanced diffusion imaging methods detected an extended reduction in FA and increased fISO along the ipsilateral white matter tracts and in the ventricles of the injured rats. These

same regions overlapped with areas with significant T2 hyperintensities and increased ventricular volume. In sham animals and subjects with smaller lateral ventricles, there were significant partial volume effect and spill over from the surrounding tissue that the apparent fISO in the smaller ventricles appeared lower; in enlarged lateral ventricles and oedemic lesions with T2 hyperintensities, apparent fISO values were higher and approached the theoretically "pure" contribution of isotropic diffusion to the total diffusion signal in the ventricles (see. Figure 3 and 6 for examples of ventricle size relationship to fISO values in ventricle voxels). Thus, the observed changes in diffusion markers are likely attributable to oedema and ventricular enlargement. Our finding of post-TBI enlargement of the ventricles or hydrocephalus matches with earlier investigation in animal TBI models,[30,76,77] and human TBI survivors.[27,78–81] Decreased cerebral volumes were present extending beyond regions with increased fISO signal, and there were no FA, ODI or NDI changes in the external capsule white matter tracts contralateral to the injury. The white matter volume loss may well correspond to the non-specific white matter degeneration commonly associated with lateral ventricle enlargement in humans (for review see[82]). White matter volume loss was also found in a mouse model of moderate-severe TBI[83] and in human TBI patients.[27,84,85] Our findings of increased FA in the thalamus are consistent with increased intra-cranial pressure and brain compression,[86] and match earlier results in an TBI model.[29]

Regression analysis of the prognostic value of the plasma cytokine marker panel at different post-injury timepoints revealed that higher plasma levels of G-CSF, IL-12p70, IL-13, M-CSF, and TNF-α and lower plasma levels of GRO/KC, MCP-1, CCL3, CCL5, and VEGF at day 7 post-injury were highly predictive of lower NDI in the ipsilateral cortex and higher NDI in the contralateral cortex at day 60 post-injury. There were no such associations for day 1 and day 3 cytokine marker panel results (Supplementary Data 2). This suggests that the day 7 immune response predicted significant neurite and neuronal loss in the cortex ipsilateral to

the injury, presumably reflecting the replacement of neurite and cell body diffusion with free water diffusion. The day 7 panel results also predicted a corresponding and proportionate gain in neurite density, as there was a significant negative correlation between ipsi- and contralateral cortical NDI values at day 60 ($r = -0.656$, P value [one-tailed] = 0.0387). This phenomenon is consistent with the interpretation of cortical reorganisation and trans-hemispherical transfer of the affected limbs' cortical map from the ipsilateral to the contralateral cortex, as is frequently observed in rodent models of unilateral TBI.[87–91] The cortical map transfer process may partially compensate for motor deficits in the limbs controlled by the affected cortex[87], although it has been shown previously that reaching deficits of the affected limbs could be rescued through timely silencing of neuronal activity in the contralateral cortex,[91] suggesting that the hemispherical transfer process can be maladaptive or pathological. Notably, there are consistent findings of a critical temporal window of this cortical map transfer process in the CCI model occurring approximately one week post-injury: the peak contralateral cortical response to affected limb, as detected by functional autoradiography[88] and sensory-evoked functional MRI cortical electrical activity recordings[90] were both seen between 4 to 7 days post-injury.[88,90] As noted above, contralateral cortical silencing could rescue affected limbs' motor impairment only when performed approximately one week post-injury.[91]

Our finding that only day 7 and not day 1, 3, or 60 plasma cytokine marker panel results had significant predictive power for the outcome of the cortical reorganisation and trans-hemispherical transfer process (as indicated by diffusion MRI signals) is thus consistent with prior literature on the relevant temporal window, which may have some implication for timely intervention in the rehabilitation process. Our results also provide evidence that systemic or neural immune responses were associated with the outcome of the interhemispheric transfer process and that early/subacute peripheral inflammatory markers can have a time-dependent

prognostic value for the subsequent neuromodulation, reorganisation, functional recovery, and repair post-TBI.

Regression analysis showed that the day 60 cytokine marker panel results were significantly associated with the fISO value in the cerebral ventricles and the number of tractography streamlines connected to the contralateral LPAC (whose NDI relation with cytokine markers at day 7 post-injury was discussed previously) of TBI animals. Of particular interest, we note that high levels of IL-1β and low levels of GM-CSF and CCL3 were associated with higher fISO in the ventricles at day 60. Higher plasma levels of IL-12p70, M-CSF, and CCL5, and lower plasma levels of IL-1β, IL-6, GM-CSF, G-CSF, and TNF-α at day 60 post-injury were associated with higher number of tractography streamlines connected to the contralateral LPAC. IL-1β, GM-CSF and CCL3 were significantly elevated in TBI animals' plasma between day 3 and day 60 post-injury. These associations seem consistent with the markers' known roles and the neuropathology of ventricle enlargement after TBI. As previously discussed, ventricle enlargement is a common feature in animal[76,77] and human[78–81] TBI, and acutely (within 24 hours post-injury) high levels of IL-1$\beta$ were associated with poorer outcomes in human TBI.[63] Furthermore, pharmacological blockade of IL-1$\beta$ function was beneficial in a mouse TBI model.[58] On the other hand, IL-7, CCL3, and GM-CSF have anti-inflammatory and neuroprotective functions,[69–72] which we suppose mitigated against ventricular enlargement in our TBI group. With regards to the markers associated with the number of tractography streamlines connected to the contralateral LPAC in TBI animals, elevated levels of IL-6 were associated with increased risk of respiratory distress,[92,93] of IL-6, IL-1$\beta$ and TNF-α were associated with increased mortality risk,[63,94] and of IL-1$\beta$, TNF-α, IFN-γ, IL-12p70, and IL-6 were associated with unfavourable outcomes,[63,95] in TBI patients. In general, lower levels of day 60 post-injury markers, previously associated with death or unfavourable outcomes in TBI patients, in this study's TBI animals were associated with more

retained tractography streamlines to the contralateral LPAC. It is likely that the individual variation among TBI animals in the number of contralateral LPAC's tractography streamlines were due to white matter tract degeneration rather than neural plasticity associated with the trans-hemispherical cortical transfer process discussed previously; there was no difference between sham and TBI animals for the number of contralateral LPAC streamlines and there was no correlation between the contralateral cortex NDI and the number of tractography streamlines connected to the same cortex. The NDI of ipsi- and contra-lateral cortices were negatively correlated with one another, on the other hand.

## 5 Conclusion

This study demonstrated the plasma cytokine marker patterns in the sub-acute/chronic phase after TBI are suggestive of predominantly restorative functions from approximately day 3 post-injury onwards in the present rat model. The conclusion of an acute phase of inflammatory responses measured in blood was marked by decreased plasma levels of pro-inflammatory markers, and the subsequent recovery phase was dominated by elevated levels of IL-1$\beta$ and several other neuroprotective cytokines and chemokines. Our advanced diffusion MRI methods detected features consistent with neuromodulation, reorganisation, and trans-hemispherical cortical map transfer after the injury. The day 7 plasma inflammatory marker panel was significantly predictive of the outcome of this reorganisation process. Day 60 inflammatory marker levels were associated with the degree of ventricle enlargement and generalised neuronal and white matter loss. Thus, we see evidence for a temporally constrained prognostic value of plasma inflammatory markers for the later outcome of post-TBI damage, repair, and recovery. These findings may suggest a therapeutic window for anti-inflammatory interventions aiming to ameliorate the clinical outcome after TBI.

## Acknowledgement

This research was supported by Motor Accident Insurance Commission (MAIC), The Queensland Government, Australia (grant number: 2014000857). We acknowledge the supports from the Queensland NMR Network and the National Imaging Facility (a National Collaborative Research Infrastructure Strategy capability) for the operation of 9.4T T MRI and the computational resources at the Centre for Advanced Imaging, the University of Queensland.

## References


1. Nguyen, R. *et al.* The International Incidence of Traumatic Brain Injury: A Systematic Review and Meta-Analysis. *Can. J. Neurol. Sci. / J. Can. des Sci. Neurol.* **43**, 774–785 (2016).

2. Menon, D. K., Schwab, K., Wright, D. W. & Maas, A. I. Position statement: Definition of traumatic brain injury. *Arch. Phys. Med. Rehabil.* **91**, 1637–1640 (2010).

3. McNett, M. A Review of the Predictive Ability of Glasgow Coma Scale Scores in Head-Injured Patients. *J. Neurosci. Nurs.* **39**, 68–75 (2007).

4. Hutchinson, E. B., Schwerin, S. C., Avram, A. V., Juliano, S. L. & Pierpaoli, C. Diffusion MRI and the detection of alterations following traumatic brain injury. *J. Neurosci. Res.* **96**, 612–625 (2018).

5. Loane, D. J. & Byrnes, K. R. Role of microglia in neurotrauma. *Neurotherapeutics* **7**, 366–377 (2010).

6. Harris, N. G., Verley, D. R., Gutman, B. A. & Sutton, R. L. Bi-directional changes in fractional anisotropy after experiment TBI: Disorganization and reorganization? *Neuroimage* **133**, 129–143 (2016).

7. Ramlackhansingh, A. F. *et al.* Inflammation after trauma: Microglial activation and traumatic brain injury. *Ann. Neurol.* **70**, 374–383 (2011).

8. Needham, E. J. *et al.* The immunological response to traumatic brain injury. *J. Neuroimmunol.* **332**, 112–125 (2019).

9. Chiu, C. *et al.* Neuroinflammation in an animal model of TBI. *J. Neurosci. methods* **272**, 38–49 (2016).

10. Blennow, K. *et al.* Traumatic brain injuries. *Nat. Rev. Dis. Prim.* **2**, 16084 (2016).

11. Woodcock, T. & Morganti-Kossmann, M. C. The role of markers of inflammation in traumatic brain injury. *Front. Neurol.* **4 MAR**, 1–18 (2013).

12. Zetterberg, H. & Blennow, K. Fluid biomarkers for mild traumatic brain injury and related conditions. *Nat. Rev. Neurol.* **12**, 563–574 (2016).

13. Vos, P. E. *et al.* Glial and neuronal proteins in serum predict outcome after severe traumatic brain injury. *Neurology* **62**, 1303–1310 (2004).

14. Chabok, S. Y. *et al.* Neuron-specific enolase and S100BB as outcome predictors in severe diffuse axonal injury. *J. Trauma Acute Care Surg.* **72**, 1654–1657 (2012).

15. Mercier, E. *et al.* Predictive value of S-100 protein for prognosis in patients with moderate and severe traumatic brain injury: systematic review and meta-analysis. *BMJ* **346**, f1757–f1757 (2013).

16. McDonald, S. J., Sun, M., Agoston, D. V. & Shultz, S. R. The effect of concomitant peripheral injury on traumatic brain injury pathobiology and outcome. *J. Neuroinflammation* **13**, 90 (2016).

17. Rowland, B. *et al.* Acute Inflammation in Traumatic Brain Injury and Polytrauma Patients Using Network Analysis. *Shock* **53**, 24–34 (2020).

18. Chen, Y. C., Mao, H., Yang, K. H., Abel, T. & Meaney, D. F. A modified controlled cortical impact technique to model mild traumatic brain injury mechanics in mice. *Front. Neurol.* **5 JUN**, 1–14 (2014).

19. Plog, B. A. *et al.* Biomarkers of traumatic injury are transported from brain to blood via the glymphatic system. *J. Neurosci.* **35**, 518–526 (2015).

20. Plog, B. A. & Nedergaard, M. Why have we not yet developed a simple blood test for TBI? *Expert Rev. Neurother.* **15**, 465–468 (2015).

21. Osier, N. D. & Dixon, C. E. The controlled cortical impact model: Applications, considerations for researchers, and future directions. *Front. Neurol.* **7**, 1–14 (2016).

22. Johnson, V. E., Meaney, D. F., Cullen, D. K. & Smith, D. H. Animal models of traumatic brain injury. in 115–128 (2015). doi:10.1016/B978-0-444-52892-6.00008-8.

23. Tajiri, N. *et al.* Suppressed cytokine expression immediatey following traumatic brain injury in neonatal rats indicates an expeditious endogenous anti-inflammatory response. *Brain Res.* **1559**, 65–71 (2014).

24. Das, M. *et al.* Lateral fluid percussion injury of the brain induces CCL20 inflammatory chemokine expression in rats. *J. Neuroinflammation* **8**, 148 (2011).

25. Wallace, E. J., Mathias, J. L. & Ward, L. Diffusion tensor imaging changes following mild, moderate and severe adult traumatic brain injury: a meta-analysis. *Brain Imaging Behav.* **12**, 1607–1621 (2018).

26. Hulkower, M. B., Poliak, D. B., Rosenbaum, S. B., Zimmerman, M. E. & Lipton, M. L. A Decade of DTI in Traumatic Brain Injury: 10 Years and 100 Articles Later. *Am. J. Neuroradiol.* **34**, 2064–2074 (2013).

27. Mohamed, A. Z., Cumming, P. & Nasrallah, F. A. White Matter Alterations Are Associated With Cognitive Dysfunction Decades After Moderate-to-Severe Traumatic Brain Injury and/or Posttraumatic Stress Disorder. *Biol. Psychiatry Cogn. Neurosci. Neuroimaging* 1–10 (2021) doi:10.1016/j.bpsc.2021.04.014.

28. MACDONALD, C. *et al.* Detection of traumatic axonal injury with diffusion tensor imaging in a mouse model of traumatic brain injury. *Exp. Neurol.* **205**, 116–131 (2007).

29. Mohamed, A. Z. *et al.* Evaluating spatiotemporal microstructural alterations following

diffuse traumatic brain injury. *NeuroImage Clin.* **25**, 102136 (2020).

30. Mohamed, A. Z., Cumming, P. & Nasrallah, F. A. Traumatic brain injury augurs ill for prolonged deficits in the structural-functional integrity of the male rat brain following controlled cortical impact injury. *Sci. ReportsRepo* **In Press**, (2021).

31. Soni, N., Mohamed, A. Z., Kurniawan, N. D., Borges, K. & Nasrallah, F. Diffusion Magnetic Resonance Imaging Unveils the Spatiotemporal Microstructural Gray Matter Changes following Injury in the Rodent Brain. *J. Neurotrauma* **36**, 1306–1317 (2019).

32. Pierpaoli, C. & Basser, P. J. Toward a quantitative assessment of diffusion anisotropy. *Magn. Reson. Med.* **36**, 893–906 (1996).

33. Beaulieu, C. The Biological Basis of Diffusion Anisotropy. in *Diffusion MRI* 105–126 (Elsevier, 2009). doi:10.1016/B978-0-12-374709-9.00006-7.

34. Zhang, H., Schneider, T., Wheeler-Kingshott, C. A. & Alexander, D. C. NODDI: Practical in vivo neurite orientation dispersion and density imaging of the human brain. *Neuroimage* **61**, 1000–1016 (2012).

35. Wang, N. *et al.* Neurite orientation dispersion and density imaging of mouse brain microstructure. *Brain Struct. Funct.* **224**, 1797–1813 (2019).

36. Gupte, R., Brooks, W., Vukas, R., Pierce, J. & Harris, J. Sex Differences in Traumatic Brain Injury: What We Know and What We Should Know. *J. Neurotrauma* **36**, 3063–3091 (2019).

37. Rorden, C. & Brett, M. Stereotaxic display of brain lesions. *Behav. Neurol.* **12**, 191–200 (2000).

38. Tustison, N. J. *et al.* N4ITK: Improved N3 Bias Correction. *IEEE Trans. Med. Imaging* **29**, 1310–1320 (2010).

39. Avants, B. B. *et al.* The Insight ToolKit image registration framework. *Front. Neuroinform.* **8**, 1–13 (2014).

40. Chou, N., Wu, J., Bai Bingren, J., Qiu, A. & Chuang, K.-H. Robust automatic rodent brain extraction using 3-D pulse-coupled neural networks (PCNN). *IEEE Trans. Image Process.* **20**, 2554–2564 (2011).

41. Barrière, D. A. *et al.* The SIGMA rat brain templates and atlases for multimodal MRI data analysis and visualization. *Nat. Commun.* **10**, 1–13 (2019).

42. Kim, J. *et al.* Structural consequences of diffuse traumatic brain injury: a large deformation tensor-based morphometry study. *Neuroimage* **39**, 1014–26 (2008).

43. Brett, M., Leff, A. P., Rorden, C. & Ashburner, J. Spatial normalization of brain images with focal lesions using cost function masking. *Neuroimage* **14**, 486–500 (2001).

44. Avants, B. B., Epstein, C. L., Grossman, M. & Gee, J. C. Symmetric diffeomorphic image registration with cross-correlation: evaluating automated labeling of elderly and neurodegenerative brain. *Med. Image Anal.* **12**, 26–41 (2008).

45. Tariq, M., Schneider, T., Alexander, D. C., Gandini Wheeler-Kingshott, C. A. & Zhang, H. Bingham-NODDI: Mapping anisotropic orientation dispersion of neurites using diffusion MRI. *Neuroimage* **133**, 207–223 (2016).

46. Szafer, A., Zhong, J. & Gore, J. C. Theoretical model for water diffusion in tissues. *Magn. Reson. Med.* **33**, 697–712 (1995).

47. Christiaens, D. *et al.* Global tractography of multi-shell diffusion-weighted imaging data using a multi-tissue model. *Neuroimage* **123**, 89–101 (2015).

48. Jeurissen, B., Tournier, J. D., Dhollander, T., Connelly, A. & Sijbers, J. Multi-tissue

constrained spherical deconvolution for improved analysis of multi-shell diffusion MRI data. *Neuroimage* **103**, 411–426 (2014).

49. Tournier, J. D., Calamante, F. & Connelly, A. MRtrix: Diffusion tractography in crossing fiber regions. *Int. J. Imaging Syst. Technol.* **22**, 53–66 (2012).

50. Dhollander, T., Raffelt, D. & Connelly, A. Unsupervised 3-tissue response function estimation from single-shell or multi-shell diffusion MR data without a co-registered T1 image Predicting stroke impairment using machine learning techniques View project A novel sparse partial correlation method fo. *ISMRM Work. Break. Barriers Diffus. MRI* **35**, 1–2 (2016).

51. Dhollander, T., Mito, R., Raffelt, D. & Connelly, A. Improved white matter response function estimation for 3-tissue constrained spherical deconvolution. *Proc. Intl. Soc. Mag. Reson. Med* 555 (2019).

52. Anderson, M. J. & Robinson, J. Permutation Tests for Linear Models. *Aust. N. Z. J. Stat.* **43**, 75–88 (2001).

53. Winkler, A. M., Ridgway, G. R., Webster, M. A., Smith, S. M. & Nichols, T. E. Permutation inference for the general linear model. *Neuroimage* **92**, 381–397 (2014).

54. Smith, S. M. & Nichols, T. E. Threshold-free cluster enhancement: Addressing problems of smoothing, threshold dependence and localisation in cluster inference. *Neuroimage* **44**, 83–98 (2009).

55. Ashburner, J. & Friston, K. J. Morphometry. in *Human Brain Function* (eds. Frackowiak, R. S. J. et al.) 707–722 (Academic Press, 2003). doi:10.1016/B978-0-12-264841-0.X5000-8.

56. Griffin, W. S. T. *et al.* Microglial interleukin-lα expression in human head injury:

Correlations with neuronal and neuritic β-amyloid precursor protein expression. *Neurosci. Lett.* **176**, 133–136 (1994).

57. Hutchinson, P. J. *et al.* Inflammation in Human Brain Injury: Intracerebral Concentrations of IL-1 α , IL-1 β , and Their Endogenous Inhibitor IL-1ra. *J. Neurotrauma* **24**, 1545–1557 (2007).

58. Newell, E. A. *et al.* Combined blockade of interleukin-1α and -1β signaling protects mice from cognitive dysfunction after traumatic brain injury. *eNeuro* **5**, 1–15 (2018).

59. Fan, L. *et al.* Experimental brain injury induces expression of interleukin-1β mRNA in the rat brain. *Mol. Brain Res.* **30**, 125–130 (1995).

60. Kamm, K., VanderKolk, W., Lawrence, C., Jonker, M. & Davis, A. T. The effect of traumatic brain injury upon the concentration and expression of interleukin-1β and interleukin-10 in the rat. *J. Trauma - Inj. Infect. Crit. Care* **60**, 152–157 (2006).

61. Rider, P. *et al.* IL-1α and IL-1β Recruit Different Myeloid Cells and Promote Different Stages of Sterile Inflammation. *J. Immunol.* **187**, 4835–4843 (2011).

62. Bettcher, B. M. *et al.* Cerebrospinal Fluid and Plasma Levels of Inflammation Differentially Relate to CNS Markers of Alzheimer's Disease Pathology and Neuronal Damage. *J. Alzheimer's Dis.* **62**, 385–397 (2018).

63. Di Battista, A. P. *et al.* Inflammatory cytokine and chemokine profiles are associated with patient outcome and the hyperadrenergic state following acute brain injury. *J. Neuroinflammation* **13**, 1–14 (2016).

64. Diamond, M. L. *et al.* IL-1β associations with posttraumatic epilepsy development: A genetics and biomarker cohort study. *Epilepsia* **55**, 1109–1119 (2014).

65. Casault, C. *et al.* Cytokine Responses in Severe Traumatic Brain Injuy: Where There

Is Smoke, Is There Fire? *Neurocrit. Care* **30**, 22–32 (2019).

66. Krukowski, K. *et al.* Traumatic brain injury in aged mice induces chronic microglia activation, synapse loss, and complement-dependent memory deficits. *Int. J. Mol. Sci.* **19**, 1–17 (2018).

67. Utagawa, A., Truettner, J. S., Dietrich, W. D. & Bramlett, H. M. Systemic inflammation exacerbates behavioral and histopathological consequences of isolated traumatic brain injury in rats. *Exp. Neurol.* **211**, 283–291 (2008).

68. Hang, C. H. *et al.* Effect of systemic LPS injection on cortical NF-κB activity and inflammatory response following traumatic brain injury in rats. *Brain Res.* **1026**, 23–32 (2004).

69. Chio, C. C. *et al.* Exercise attenuates neurological deficits by stimulating a critical HSP70/NF-KB/IL-6/synapsin I axis in traumatic brain injury rats. *J. Neuroinflammation* **14**, 1–18 (2017).

70. Nishihara, T. *et al.* Subcutaneous injection containing IL-3 and GM-CSF ameliorates stab wound-induced brain injury in rats. *Exp. Neurol.* **229**, 507–516 (2011).

71. Shultz, S. R. *et al.* Granulocyte-macrophage colony-stimulating factor is neuroprotective in experimental traumatic brain injury. *J. Neurotrauma* **31**, 976–983 (2014).

72. Williams, A. M. *et al.* Early single-dose exosome treatment improves neurologic outcomes in a 7-day swine model of traumatic brain injury and hemorrhagic shock. *J. Trauma Acute Care Surg.* **89**, 388–396 (2020).

73. Thelin, E. P. *et al.* Elucidating Pro-Inflammatory Cytokine Responses after Traumatic Brain Injury in a Human Stem Cell Model. *J. Neurotrauma* **35**, 341–352 (2018).

74. Edalatfar, M. *et al.* Biofluid Biomarkers in Traumatic Brain Injury: A Systematic Scoping Review. *Neurocrit. Care* (2021) doi:10.1007/s12028-020-01173-1.

75. Jiang, L. *et al.* Breviscapine reduces neuronal injury caused by traumatic brain injury insult: partly associated with suppression of interleukin-6 expression. *Neural Regen. Res.* **12**, 90 (2017).

76. Dixon, C. E. *et al.* One-year study of spatial memory performance, brain morphology, and cholinergic markers after moderate controlled cortical impact in rats. *J. Neurotrauma* **16**, 109–122 (1999).

77. Zhao, J., Chen, Z., Xi, G., Keep, R. F. & Hua, Y. Deferoxamine Attenuates Acute Hydrocephalus After Traumatic Brain Injury in Rats. *Transl. Stroke Res.* **5**, 586–594 (2014).

78. Edna, T.-H. & Cappelen, J. Return to work and social adjustment after traumatic head injury. *Acta Neurochir. (Wien).* **85**, 40–43 (1987).

79. Gale, S. D., Johnson, S. C., Bigler, E. D. & Blatter, D. D. Nonspecific white matter degeneration following traumatic brain injury. *J. Int. Neuropsychol. Soc.* **1**, 17–28 (1995).

80. ANDERSON, C. V., WOOD, D.-M. G., BIGLER, E. D. & BLATTER, D. D. Lesion Volume, Injury Severity, and Thalamic Integrity following Head Injury. *J. Neurotrauma* **13**, 59–65 (1996).

81. Poca, M. A. *et al.* Ventricular Enlargement after Moderate or Severe Head Injury: A Frequent and Neglected Problem. *J. Neurotrauma* **22**, 1303–1310 (2005).

82. Levine, B. *et al.* In vivo characterization of traumatic brain injury neuropathology with structural and functional neuroimaging. *J. Neurotrauma* **23**, 1396–1411 (2006).

83. Pischiutta, F. *et al.* Single severe traumatic brain injury produces progressive pathology with ongoing contralateral white matter damage one year after injury. *Exp. Neurol.* **300**, 167–178 (2018).

84. Brezova, V. *et al.* Prospective longitudinal MRI study of brain volumes and diffusion changes during the first year after moderate to severe traumatic brain injury. *NeuroImage Clin.* **5**, 128–140 (2014).

85. Cole, J. H. *et al.* Spatial patterns of progressive brain volume loss after moderate-severe traumatic brain injury. *Brain* **141**, 822–836 (2018).

86. Osuka, S. *et al.* Elevated diffusion anisotropy in gray matter and the degree of brain compression. *J. Neurosurg.* **117**, 363–371 (2012).

87. Holschneider, D. P., Guo, Y., Wang, Z., Roch, M. & Scremin, O. U. Remote brain network changes after unilateral cortical impact injury and their modulation by acetylcholinesterase inhibition. *J. Neurotrauma* **30**, 907–919 (2013).

88. Harris, N. G., Chen, S. F. & Pickard, J. D. Cortical reorganization after experimental traumatic brain injury: A functional autoradiography study. *J. Neurotrauma* **30**, 1137–1146 (2013).

89. Le Prieult, F., Thal, S. C., Engelhard, K., Imbrosci, B. & Mittmann, T. Acute Cortical Transhemispheric Diaschisis after Unilateral Traumatic Brain Injury. *J. Neurotrauma* **34**, 1097–1110 (2017).

90. Verley, D. R. *et al.* Remote Changes in Cortical Excitability after Experimental Traumatic Brain Injury and Functional Reorganization. *J. Neurotrauma* **35**, 2448–2461 (2018).

91. Verley, D. R., Torolira, D., Hessell, B. A., Sutton, R. L. & Harris, N. G. Cortical

Neuromodulation of Remote Regions after Experimental Traumatic Brain Injury Normalizes Forelimb Function but is Temporally Dependent. *J. Neurotrauma* **36**, 789–801 (2019).

92. Woiciechowsky, C. *et al.* Early il-6 plasma concentrations correlate with severity of brain injury and pneumonia in brain-injured patients. *J. Trauma* **52**, 339–345 (2002).

93. Aisiku, I. P. *et al.* Plasma cytokines IL-6, IL-8, and IL-10 are associated with the development of acute respiratory distress syndrome in patients with severe traumatic brain injury. *Crit. Care* **20**, 1–10 (2016).

94. Maier, B. *et al.* Early versus late onset of multiple organ failure is associated with differing patterns of plasma cytokine biomarker expression and outcome after severe trauma. *Shock* **28**, 668–674 (2007).

95. Nwachuku, E. L. *et al.* Time course of cerebrospinal fluid inflammatory biomarkers and relationship to 6-month neurologic outcome in adult severe traumatic brain injury. *Clin. Neurol. Neurosurg.* **149**, 1–5 (2016).

## Figure captions

Table 1: Results of Principal Component Regression (PCR) predicting Neurite Density Index (NDI) in the contralateral cortical area region-of-interest (ROI) from the plasma cytokine panel at day 7 post-injury.

Table 2: Results of Principal Component Regression (PCR) predicting Neurite Density Index (NDI) in the ipsilateral cortical area region-of-interest (ROI) from the plasma cytokine panel at day 7 post-injury.

Table 3: Results of Principal Component Regression (PCR) predicting isotropic diffusion fraction (fISO) in the ventricle region-of-interest (ROI) from the plasma cytokine panel at day 60 post-injury.

Table 4: Results of Principal Component Regression (PCR) predicting the number of tractography streamlines connected to the contralateral lateral parietal associative cortex (LPAC) from the plasma cytokine panel at day 60 post-injury.

Table 5: One-way analysis of variance and post-hoc statistical test assessing the effects of ipsi- versus contra-lateral and TBI effects on the number of tractography streamlines connected to the lateral parietal associative cortex.

Figure 1: Plasma levels of cytokine markers: interleukins- (IL-) IL-12p70, IL-1$\alpha$, IL-1$\beta$, IL-7, macrophage colony-stimulating factor (M-CSF), chemokine (C-C motif) ligands- (CCL) 3, CCL5, growth-regulated oncogene/keratinocyte chemoattractant (GRO-KC), granulocyte-macrophage colony-stimulating factor (GM-CSF). Unpaired Mann-Whitney tests of sham (n = 6, blue solid lines and circle symbols) vs. traumatic brain injury (n = 8, red broken lines and square symbols), multiple comparison corrections were performed using false discovery rate (FDR) thresholded at the desired FDR (Q) < 0.1. * Q value < 0.1.

Figure 2: Plasma levels of cytokine markers: interleukins- (IL-) IL-6, IL-19, IL-13, IL-17$\alpha$, IL-2, IL-4, IL-5, granulocyte colony-stimulating factor (G-CSF), interferon gamma (IFN-$\gamma$). Unpaired Mann-Whitney tests sham (n = 6, blue solid lines and circle symbols) vs. traumatic brain injury (n = 8, red broken lines and square symbols), multiple comparison corrections were performed using false discovery rate (FDR) thresholded at the desired FDR (Q) < 0.1.

Figure 3: Examples of T2-weighted structural image, global tractography streamlines, neurite density index (NDI), and isotropic diffusion volume fraction (fISO) of two animals from each of sham, traumatic brain injured (TBI) animals with very high plasma cytokine levels (those seen in Figure 2), and other TBI animals without the very high cytokine levels. Middle slices in each row contained the lateral parietal associative cortex.

Figure 4: Voxel-wise statistical analysis results of diffusion tensor imaging Fractional Anisotropy (FA) and neurite orientation dispersion and density imaging Orientation Dispersion Index (ODI), Neurite Density Index (NDI), isotropic diffusion fraction (fISO), and the tensor-based morphometry Jacobian Index (JI) of controlled cortical impacted animals (n = 8) compared to sham animals (n = 6). Image displayed as statistical map overlaid on averaged and registered corresponding DTI and NODDI metric maps corresponding to the statistical maps (FA, ODI, NDI, and fISO results) and structural template (JI result). Corresponding grey scale maps for each of the averaged FA, ODI, NDI, and fISO image were provided. Statistical maps thresholded at P value < 0.05 (two-tailed), unpaired two sample t test, implemented as permutation inference for the general linear model, corrected for multiple comparisons with mass-based FSL's threshold-free cluster enhancement (TFCE). Red anatomical orientation marker L = Left, R = Right.

Figure 5: (a) summary of the total number of global tractography streamlines connected to the ipsi- and contra-lateral lateral parietal associative cortex (LPAC), post-hoc Fisher's least significant difference test of two-way analysis of variance, ** P value < 0.01, correlation

between (b) Neurite Density Index (NDI) quantified from the ipsi- and contra-lateral cortical areas, (c) NDI of contralateral cortical area and the number of streamlines connected to the contralateral LPAC, d) the number of streamlines connected to the ipsi- and contra-lateral LPAC.

Figure 6: Summary of trends in Neurite Density Index (NDI), isotropic diffusion fraction (fISO) changes and the corresponding plasma cytokine biomarker changes in the traumatic brain injured animals at day 60 post-injury.

Supplementary Figure 1: Plasma levels of cytokine markers: chemokine (C-C motif) ligands-(CCL) CCL20, tumour necrosis factor alpha (TNF-$\alpha$), monocyte chemoattractant protein-1 (MCP-1), interleukin 18 (IL-18), and vascular endothelial growth factor (VEGF).

Supplementary Figure 2: Regions-of-interest (ROIs) selected and used for ROI-based quantification of NODDI metrics used for principal component regression analysis. ROI defined and extracted from voxel-wise multiple linear regression predicting Neurite Density Index (NDI), isotropic diffusion fraction (fISO) outcomes at 60 days post-injury using each TBI rat's cytokine marker panels at each time point. Statistical maps thresholded at P value < 0.05 (two-tailed), unpaired two sample t-test, implemented as permutation inference for the general linear model, corrected for multiple comparisons with mass-based FSL's threshold-free cluster enhancement (TFCE).

Supplementary Data 2: Results of Principal Component Regression Analyses predicting Neurite Density Index (NDI) in the contralateral and ipsilateral cortical area region-of-interest (ROI) and isotropic diffusion fraction (fISO) in the ventricle ROI from the plasma cytokine panel at days 1, 3, 7, and 60 post-injury that returned non-significant results.

Dependent variable: NDI in the contralateral cortical area ROI

| **Model** | | | | | |
|---|---|---|---|---|---|
| **Analysis of Variance** | **SS** | **DF** | **MS** | **F (DFn, DFd)** | **P value** |

| | | | | | |
|---|---|---|---|---|---|
| Regression | 6.9 | 4 | 1.73 | F (4, 3) = 53.9 | P=0.0040 |
| Residual | 0.0961 | 3 | 0.032 | | |
| Total | 7 | 7 | | | |

**Goodness of Fit**

| | |
|---|---|
| DOF | 3 |
| R squared | 0.986 |

| **Day 7 markers as variables** | **Estimate** | **95% CI (asymptotic)** | | | **\|t\|** | **P value** | |
|---|---|---|---|---|---|---|---|
| Intercept | -2.55E+00 | -4.74E+00 | to | -3.71E-01 | 3.72 | 0.0337 | * |
| IL-6 | 7.76E-05 | 5.47E-05 | to | 1.01E-04 | 10.8 | 0.0017 | ** |
| G-CSF | 1.16E-04 | 6.65E-05 | to | 1.65E-04 | 7.46 | 0.005 | ** |
| GRO/KC | -3.60E-04 | -5.57E-04 | to | -1.62E-04 | 5.79 | 0.0102 | * |
| IFN-γ | 5.13E-05 | 3.17E-05 | to | 7.09E-05 | 8.34 | 0.0036 | ** |
| IL-19 | 1.18E-04 | 3.48E-06 | to | 2.32E-04 | 3.28 | 0.0465 | * |
| IL-12p70 | 1.61E-03 | 6.18E-04 | to | 2.61E-03 | 5.15 | 0.0142 | * |
| IL-13 | 7.79E-05 | 4.99E-05 | to | 1.06E-04 | 8.86 | 0.003 | ** |
| IL-17a | 3.42E-05 | 1.64E-05 | to | 5.21E-05 | 6.11 | 0.0088 | ** |
| IL-18 | 1.70E-05 | 1.75E-07 | to | 3.38E-05 | 3.22 | 0.0488 | * |
| IL-1α | 1.57E-03 | 5.45E-04 | to | 2.59E-03 | 4.88 | 0.0165 | * |
| IL-1β | -6.56E-05 | -2.71E-04 | to | 1.39E-04 | 1.02 | 0.3838 | ns |
| IL-2 | 2.70E-05 | 4.55E-06 | to | 4.93E-05 | 3.83 | 0.0314 | * |
| IL-4 | 3.26E-05 | 1.06E-05 | to | 5.46E-05 | 4.71 | 0.0181 | * |
| IL-5 | 6.35E-04 | 4.43E-04 | to | 8.27E-04 | 10.5 | 0.0018 | ** |
| IL-7 | 2.45E-05 | -4.12E-04 | to | 4.61E-04 | 0.179 | 0.8697 | ns |
| M-CSF | 6.11E-03 | 4.38E-03 | to | 7.84E-03 | 11.2 | 0.0015 | ** |
| MCP-1 | -1.57E-04 | -2.32E-04 | to | -8.23E-05 | 6.68 | 0.0068 | ** |
| GM-CSF | -2.36E-04 | -4.75E-04 | to | 3.09E-06 | 3.14 | 0.0516 | ns |
| CCL3 | -2.96E-04 | -3.76E-04 | to | -2.16E-04 | 11.8 | 0.0013 | ** |
| CCL20 | 3.12E-04 | -6.07E-05 | to | 6.85E-04 | 2.66 | 0.0761 | ns |
| CCL5 | -5.44E-05 | -8.49E-05 | to | -2.40E-05 | 5.7 | 0.0107 | * |
| TNF-α | 3.62E-03 | 2.63E-03 | to | 4.61E-03 | 11.7 | 0.0014 | ** |
| VEGF | -1.21E-03 | -1.92E-03 | to | -5.01E-04 | 5.43 | 0.0123 | * |

Dependent variable: NDI in the ipsilateral cortical area ROI

**Model**

| **Analysis of Variance** | **SS** | **DF** | **MS** | **F (DFn, DFd)** | **P value** |
|---|---|---|---|---|---|
| Regression | 6.82 4 | 4 | 1.71 | F (4, 3) = 28.5 | P=0.0101 |
| Residual | 0.180 3 | 3 | 0.06 | | |

| | | | |
|---|---|---|---|
| Total | 7.00 | 7 | 7 |

**Goodness of Fit**

| | |
|---|---|
| DOF | 3 |
| R squared | 0.974 |

| **Day 7 markers as variables** | **Estimate** | **95% CI (asymptotic)** | | | **\|t\|** | **P value** | |
|---|---|---|---|---|---|---|---|
| Intercept | -8.91E-01 | -3.88E+00 | to | 2.10E+00 | 0.949 | 0.4127 | ns |
| IL-6 | -1.35E-05 | -4.48E-05 | to | 1.79E-05 | 1.37 | 0.2654 | ns |
| G-CSF | -9.08E-05 | -1.58E-04 | to | -2.31E-05 | 4.27 | 0.0236 | * |
| GRO/KC | 6.24E-04 | 3.53E-04 | to | 8.94E-04 | 7.34 | 0.0052 | ** |
| IFN-γ | 3.16E-06 | -2.36E-05 | to | 2.99E-05 | 0.375 | 0.7325 | ns |
| IL-19 | 8.96E-05 | -6.66E-05 | to | 2.46E-04 | 1.83 | 0.1653 | ns |
| IL-12p70 | -1.52E-03 | -2.89E-03 | to | -1.60E-04 | 3.56 | 0.0379 | * |
| IL-13 | -4.70E-05 | -8.53E-05 | to | -8.78E-06 | 3.91 | 0.0297 | * |
| IL-17a | 1.37E-05 | -1.07E-05 | to | 3.81E-05 | 1.79 | 0.1714 | ns |
| IL-18 | -8.80E-06 | -3.18E-05 | to | 1.42E-05 | 1.22 | 0.31 | ns |
| IL-1α | -1.24E-03 | -2.64E-03 | to | 1.54E-04 | 2.83 | 0.0661 | ns |
| IL-1β | 3.92E-04 | 1.12E-04 | to | 6.73E-04 | 4.45 | 0.0211 | * |
| IL-2 | 1.32E-05 | -1.74E-05 | to | 4.38E-05 | 1.37 | 0.2639 | ns |
| IL-4 | 2.02E-05 | -9.91E-06 | to | 5.04E-05 | 2.14 | 0.1223 | ns |
| IL-5 | 7.19E-06 | -2.55E-04 | to | 2.70E-04 | 0.0872 | 0.936 | ns |
| IL-7 | 1.00E-03 | 4.07E-04 | to | 1.60E-03 | 5.35 | 0.0128 | * |
| M-CSF | -6.04E-03 | -8.41E-03 | to | -3.67E-03 | 8.1 | 0.0039 | ** |
| MCP-1 | 2.21E-04 | 1.19E-04 | to | 3.24E-04 | 6.88 | 0.0063 | ** |
| GM-CSF | 8.08E-04 | 4.81E-04 | to | 1.13E-03 | 7.86 | 0.0043 | ** |
| CCL3 | 3.57E-04 | 2.48E-04 | to | 4.67E-04 | 10.4 | 0.0019 | ** |
| CCL20 | -2.86E-06 | -5.13E-04 | to | 5.07E-04 | 0.0179 | 0.9869 | ns |
| CCL5 | 5.81E-05 | 1.65E-05 | to | 9.97E-05 | 4.45 | 0.0212 | * |
| TNF-α | -3.28E-03 | -4.63E-03 | to | -1.92E-03 | 7.71 | 0.0045 | ** |
| VEGF | 1.87E-03 | 9.00E-04 | to | 2.84E-03 | 6.13 | 0.0087 | ** |

Dependent variable: fISO in the ventricle ROI

**Model**

| **Analysis of Variance** | **SS** | **DF** | **MS** | **F (DFn, DFd)** | **P value** |
|---|---|---|---|---|---|
| Regression | 6.99 | 4 | 1.75 | F (4, 3) = 639 | P=0.0001 |
| Residual | 0.00821 | 3 | 0.003 | | |
| Total | 7 | 7 | | | |

**Goodness of Fit**

| | |
|---|---|
| DOF | 3 |
| R squared | 0.999 |

| Day 60 markers as variables | Estimate | 95% CI (asymptotic) | | | \|t\| | P value | |
|---|---|---|---|---|---|---|---|
| Intercept | -1.80E+00 | -2.19E+00 | to | -1.41E+00 | 14.8 | 0.0007 | *** |
| IL-6 | 6.21E-03 | 5.63E-03 | to | 6.79E-03 | 34.1 | <0.0001 | **** |
| G-CSF | 9.21E-03 | 8.43E-03 | to | 9.99E-03 | 37.5 | <0.0001 | **** |
| GRO/KC | -4.11E-05 | -6.48E-05 | to | -1.74E-05 | 5.51 | 0.0117 | * |
| IFN-γ | 3.62E-03 | 3.33E-03 | to | 3.91E-03 | 39.3 | <0.0001 | **** |
| IL-19 | -4.22E-04 | -6.43E-04 | to | -2.02E-04 | 6.1 | 0.0089 | ** |
| IL-12p70 | -1.35E-03 | -1.51E-03 | to | -1.18E-03 | 26 | 0.0001 | *** |
| IL-13 | 1.84E-03 | 1.62E-03 | to | 2.06E-03 | 26.4 | 0.0001 | *** |
| IL-17a | 4.53E-04 | 2.93E-04 | to | 6.13E-04 | 9.02 | 0.0029 | ** |
| IL-18 | 4.17E-05 | 3.50E-05 | to | 4.83E-05 | 20 | 0.0003 | *** |
| IL-1α | -3.27E-03 | -3.58E-03 | to | -2.96E-03 | 33.8 | <0.0001 | **** |
| IL-1β | 1.89E-05 | 2.95E-06 | to | 3.48E-05 | 3.77 | 0.0326 | * |
| IL-2 | 4.77E-04 | 3.41E-04 | to | 6.13E-04 | 11.2 | 0.0015 | ** |
| IL-4 | 1.24E-03 | 1.13E-03 | to | 1.34E-03 | 37.7 | <0.0001 | **** |
| IL-5 | -3.55E-04 | -5.64E-04 | to | -1.46E-04 | 5.41 | 0.0124 | * |
| IL-7 | 7.09E-06 | -1.02E-05 | to | 2.44E-05 | 1.31 | 0.2828 | ns |
| M-CSF | -3.37E-03 | -3.79E-03 | to | -2.94E-03 | 25.2 | 0.0001 | *** |
| MCP-1 | -1.49E-04 | -1.74E-04 | to | -1.24E-04 | 18.8 | 0.0003 | *** |
| GM-CSF | -1.57E-05 | -3.09E-05 | to | -4.71E-07 | 3.28 | 0.0464 | * |
| CCL3 | -3.04E-05 | -4.46E-05 | to | -1.62E-05 | 6.8 | 0.0065 | ** |
| CCL20 | -3.40E-04 | -4.24E-04 | to | -2.55E-04 | 12.7 | 0.001 | ** |
| CCL5 | -1.61E-03 | -1.74E-03 | to | -1.48E-03 | 40 | <0.0001 | **** |
| TNF-α | 4.04E-03 | 3.65E-03 | to | 4.43E-03 | 32.9 | <0.0001 | **** |
| VEGF | -3.05E-04 | -3.56E-04 | to | -2.53E-04 | 18.9 | 0.0003 | *** |

Dependent variable: number of streamlines through contralateral lateral parietal associative cortex

**Model**

| Analysis of Variance | SS | DF | MS | F (DFn, DFd) | P value |
|---|---|---|---|---|---|
| Regression | 6270 | 4 | 1568 | F (4, 3) = 27.7 | P=0.0105 |
| Residual | 170 | 3 | 56.6 | | |
| Total | 6440 | 7 | | | |

**Goodness of Fit**

| | |
|---|---|
| DOF | 3 |
| R squared | 0.974 |

| Day 60 markers as variables | Estimate | 95% CI (asymptotic) | | | \|t\| | P value | |
|---|---|---|---|---|---|---|---|
| Intercept | 1.08E+02 | 5.29E+01 | to | 1.64E+02 | 6.22 | 0.0084 | ** |
| IL-6 | -1.69E-01 | -2.52E-01 | to | -8.53E-02 | 6.44 | 0.0076 | ** |
| G-CSF | -2.25E-01 | -3.37E-01 | to | -1.12E-01 | 6.36 | 0.0079 | ** |
| GRO/KC | -4.50E-03 | -7.91E-03 | to | -1.09E-03 | 4.2 | 0.0247 | * |
| IFN-γ | -7.77E-02 | -1.20E-01 | to | -3.55E-02 | 5.87 | 0.0099 | ** |
| IL-19 | 5.51E-02 | 2.34E-02 | to | 8.68E-02 | 5.53 | 0.0116 | * |
| IL-12p70 | 6.09E-02 | 3.71E-02 | to | 8.47E-02 | 8.14 | 0.0039 | ** |
| IL-13 | -2.19E-02 | -5.38E-02 | to | 1.01E-02 | 2.18 | 0.1175 | ns |
| IL-17a | 3.00E-02 | 7.02E-03 | to | 5.30E-02 | 4.15 | 0.0254 | * |
| IL-18 | -2.52E-04 | -1.21E-03 | to | 7.04E-04 | 0.838 | 0.4633 | ns |
| IL-1α | 1.35E-01 | 9.09E-02 | to | 1.80E-01 | 9.7 | 0.0023 | ** |
| IL-1β | -4.42E-03 | -6.71E-03 | to | -2.13E-03 | 6.14 | 0.0087 | ** |
| IL-2 | 1.37E-02 | -5.89E-03 | to | 3.32E-02 | 2.22 | 0.1126 | ns |
| IL-4 | -5.37E-03 | -2.04E-02 | to | 9.65E-03 | 1.14 | 0.3377 | ns |
| IL-5 | 5.88E-02 | 2.88E-02 | to | 8.89E-02 | 6.23 | 0.0084 | ** |
| IL-7 | -4.14E-03 | -6.63E-03 | to | -1.66E-03 | 5.31 | 0.0131 | * |
| M-CSF | 1.94E-01 | 1.33E-01 | to | 2.56E-01 | 10.1 | 0.0021 | ** |
| MCP-1 | -7.88E-04 | -4.41E-03 | to | 2.83E-03 | 0.693 | 0.5382 | ns |
| GM-CSF | -3.26E-03 | -5.44E-03 | to | -1.07E-03 | 4.74 | 0.0178 | * |
| CCL3 | -1.38E-03 | -3.42E-03 | to | 6.67E-04 | 2.15 | 0.1213 | ns |
| CCL20 | 1.94E-02 | 7.21E-03 | to | 3.16E-02 | 5.06 | 0.0149 | * |
| CCL5 | 5.34E-02 | 3.50E-02 | to | 7.18E-02 | 9.22 | 0.0027 | ** |
| TNF-α | -8.58E-02 | -1.42E-01 | to | -2.97E-02 | 4.87 | 0.0165 | * |
| VEGF | -2.59E-03 | -9.97E-03 | to | 4.79E-03 | 1.12 | 0.3449 | ns |

| ANOVA table | SS | DF | MS | F (DFn, DFd) | P value | |
|---|---|---|---|---|---|---|
| TBI x ipsi vs. contra | 7224 | 1 | 7224 | F (1, 12) = 7.088 | P=0.0207 | * |
| TBI | 16324 | 1 | 16324 | F (1, 12) = 5.601 | P=0.0356 | * |
| ipsi vs. contra | 0.2976 | 1 | 0.2976 | F (1, 12) = 0.0002920 | P=0.9866 | ns |
| subject | 34974 | 12 | 2915 | F (12, 12) = 2.859 | P=0.0405 | * |
| Residual | 12231 | 12 | 1019 | | | |

| sham vs. TBI difference | |
|---|---|
| Mean of sham | 189.2 |
| Mean of TBI | 140.4 |
| Difference between means | 48.79 |
| SE of difference | 20.62 |
| 95% CI of difference | 3.872 to 93.71 |

| ipsi-cor vs. contra-cor difference | |
|---|---|
| Mean of ipsi-cor | 164.9 |
| Mean of contra-cor | 164.7 |
| Difference between means | 0.2083 |
| SE of difference | 12.19 |
| 95% CI of difference | -26.36 to 26.77 |

| Uncorrected Fisher's LSD | Predicted (LS) mean difference | 95.00% CI of difference | P Value | |
|---|---|---|---|---|
| **sham - TBI** | | | | |
| ipsi-cor | 81.25 | 31.82 to 130.7 | P=0.0024 | ** |
| contra-cor | 16.33 | -33.10 to 65.77 | P=0.5018 | ns |
| | | | | |
| **ipsi-cor - contra-cor** | | | | |
| sham | 32.67 | -7.495 to 72.83 | P=0.1017 | ns |
| TBI | -32.25 | -67.03 to 2.531 | P=0.0663 | ns |

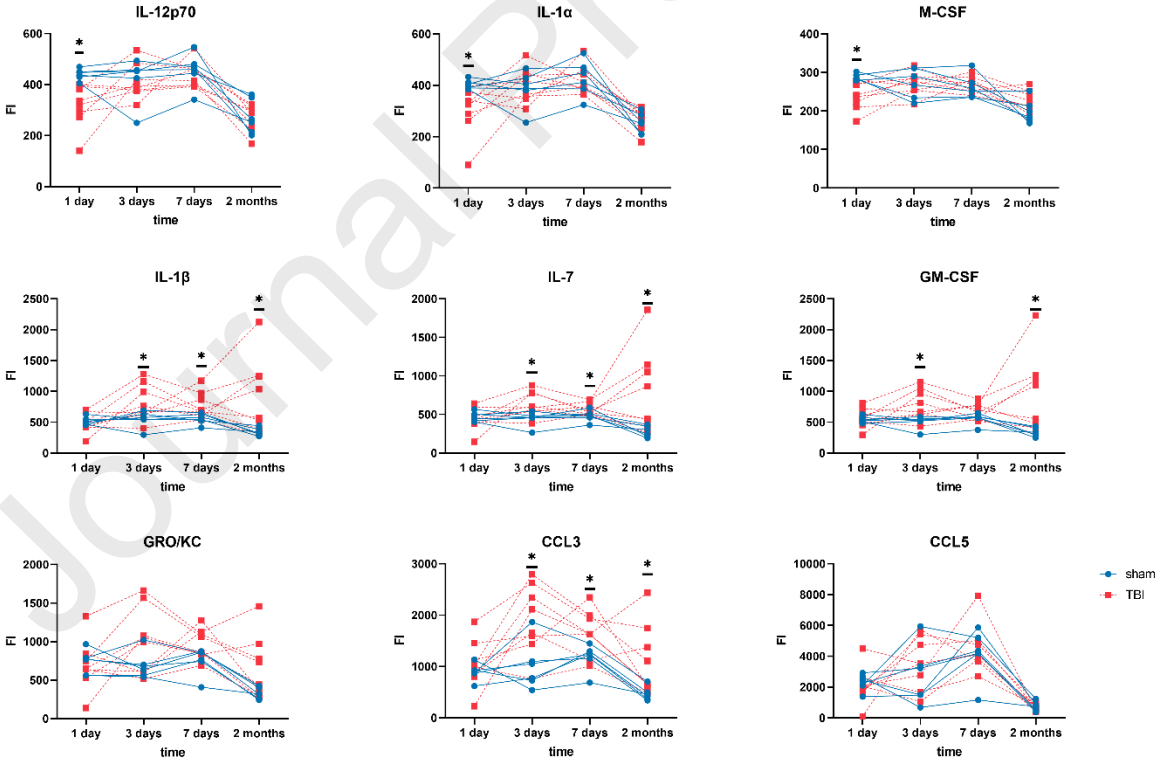

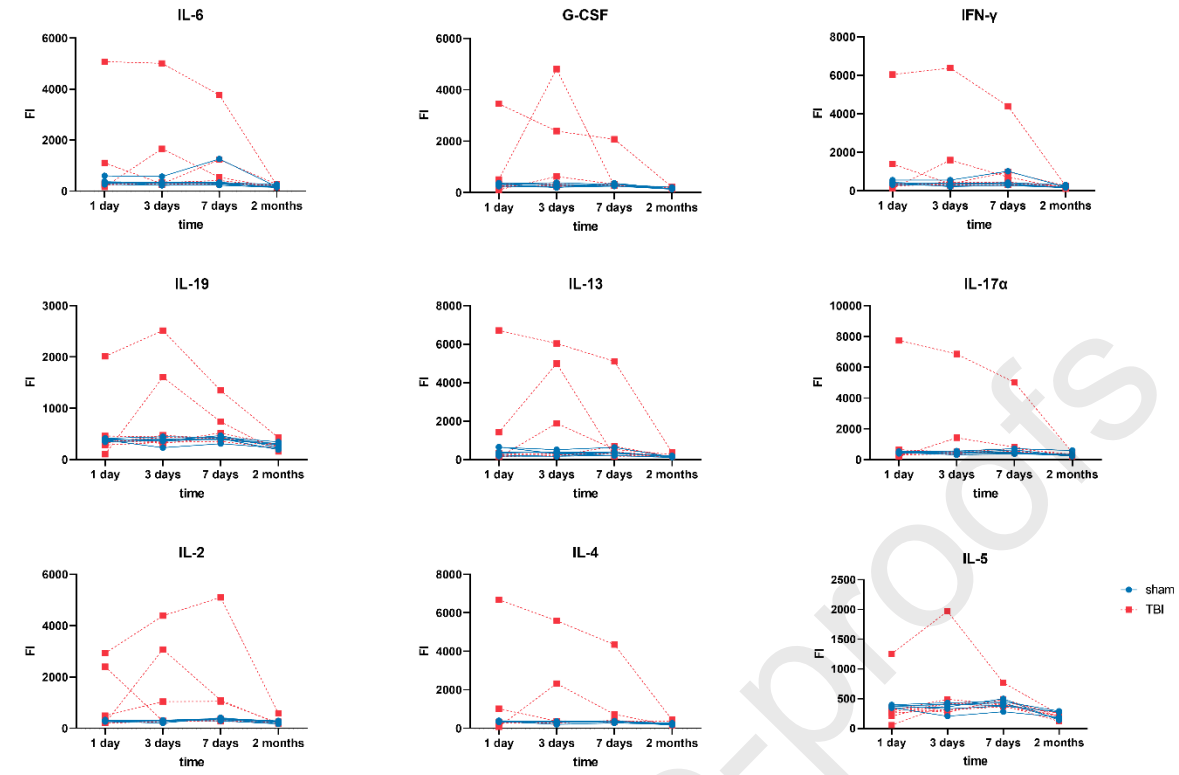
IL-6
G-CSF
IFN-γ
IL-19
IL-13
IL-17α
IL-2
IL-4
IL-5
FI
time
1 day
3 days
7 days
2 months
sham
TBI

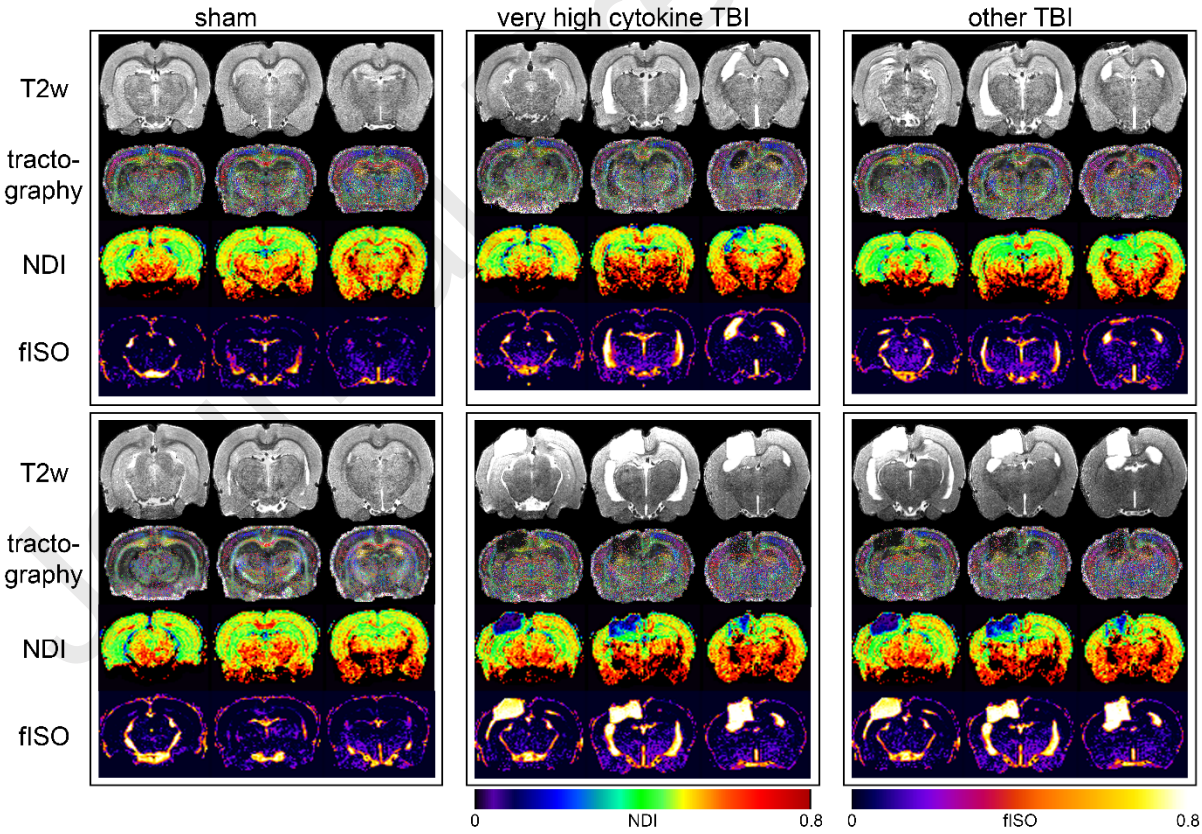
sham
very high cytokine TBI
other TBI
T2w
tracto-
graphy
NDI
fISO
0
NDI
0.8
0
fISO
0.8

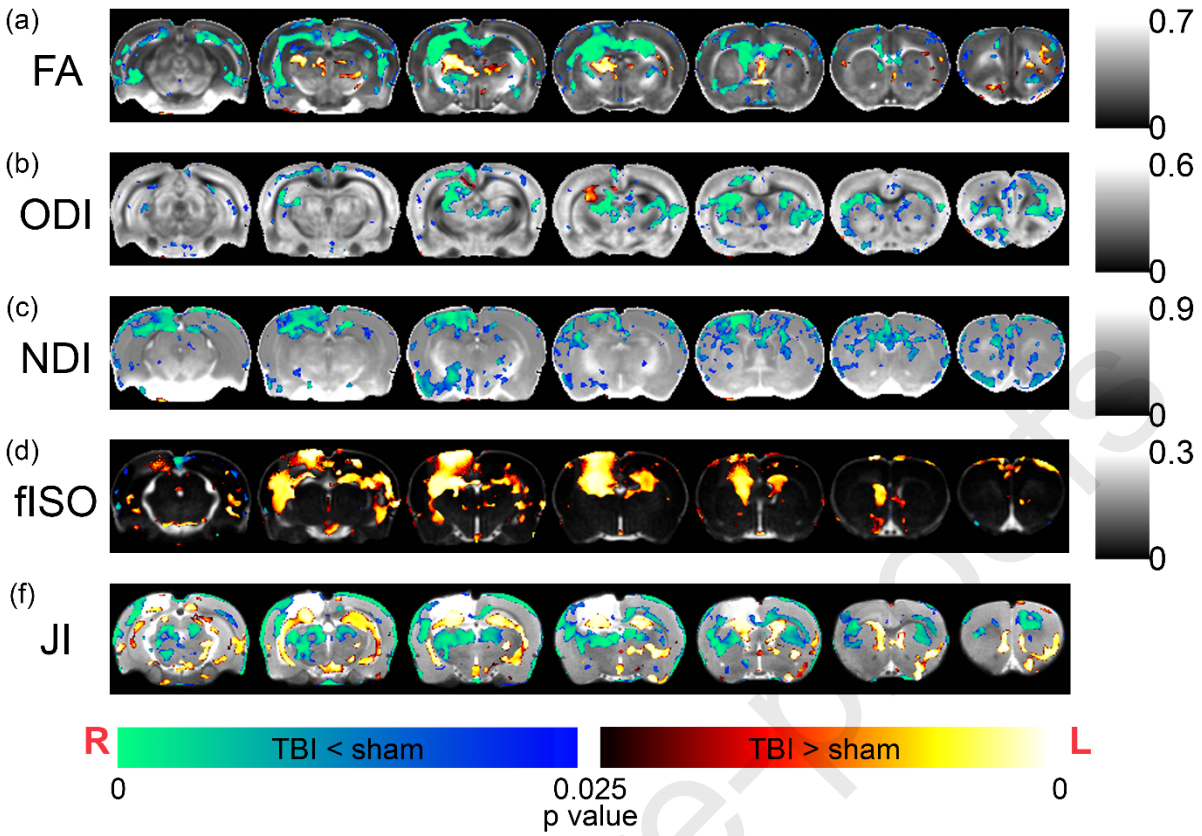


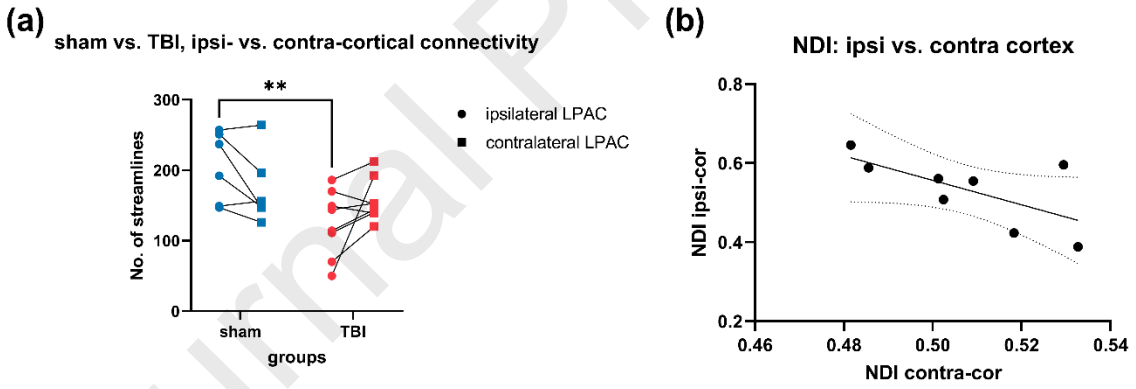





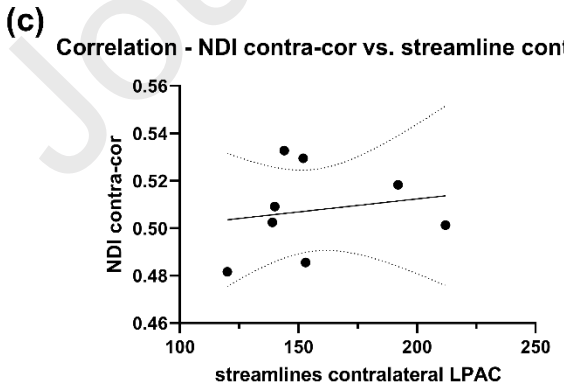


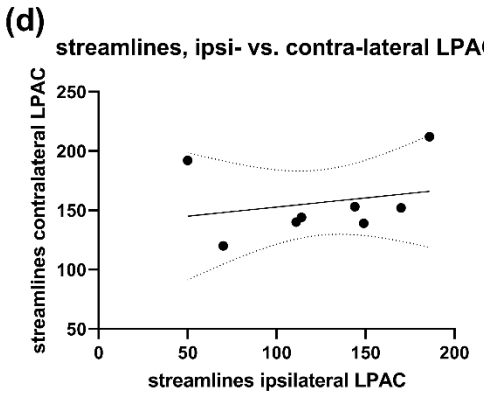

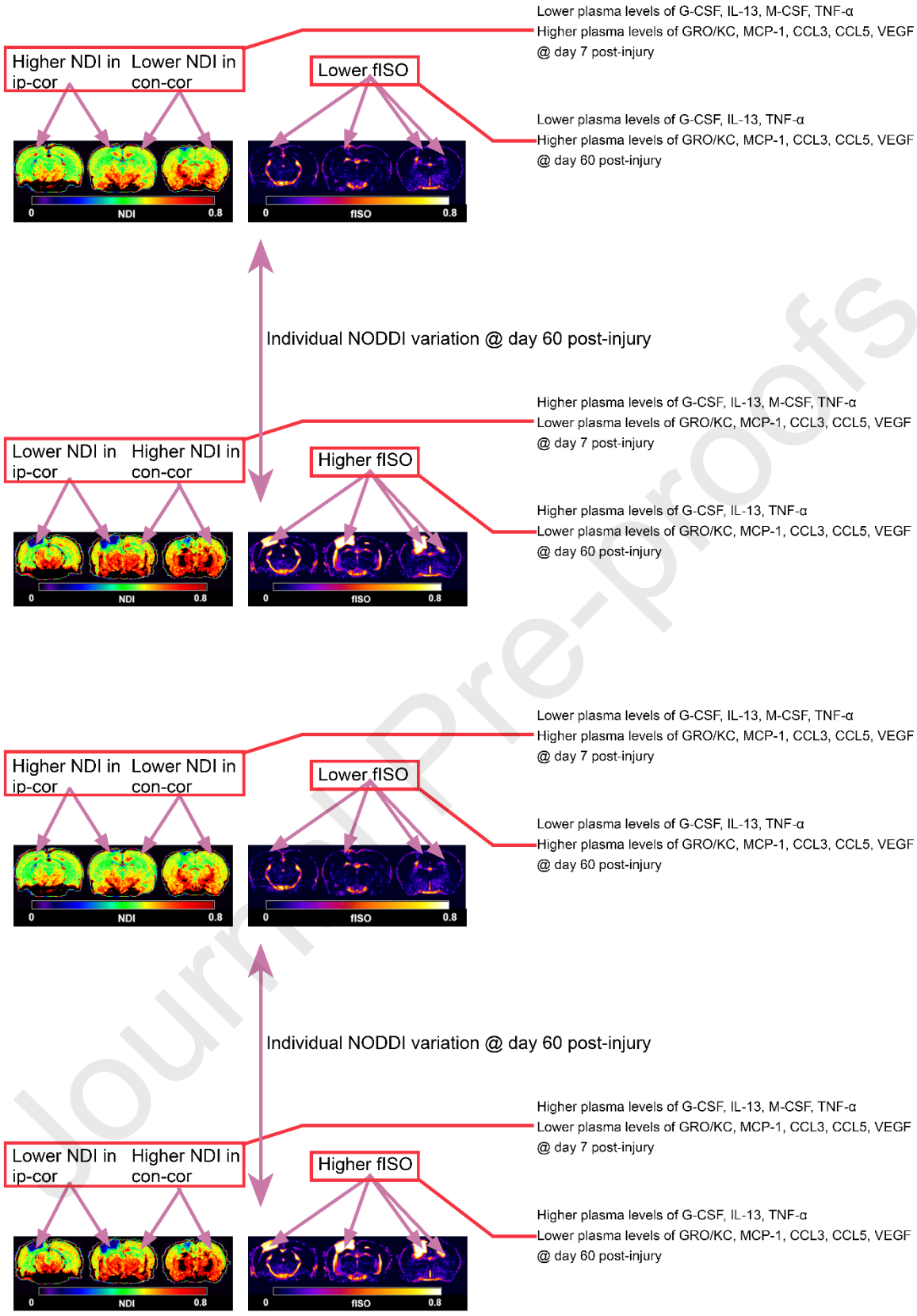
Higher NDI in ip-cor
Lower NDI in con-cor
Lower fISO
Lower plasma levels of G-CSF, IL-13, M-CSF, TNF-α
Higher plasma levels of GRO/KC, MCP-1, CCL3, CCL5, VEGF
@ day 7 post-injury
Lower plasma levels of G-CSF, IL-13, TNF-α
Higher plasma levels of GRO/KC, MCP-1, CCL3, CCL5, VEGF
@ day 60 post-injury
0
NDI
0.8
0
fISO
0.8
Individual NODDI variation @ day 60 post-injury
Lower NDI in ip-cor
Higher NDI in con-cor
Higher fISO
Higher plasma levels of G-CSF, IL-13, M-CSF, TNF-α
Lower plasma levels of GRO/KC, MCP-1, CCL3, CCL5, VEGF
@ day 7 post-injury
Higher plasma levels of G-CSF, IL-13, TNF-α
Lower plasma levels of GRO/KC, MCP-1, CCL3, CCL5, VEGF
@ day 60 post-injury
Higher NDI in ip-cor
Lower NDI in con-cor
Lower fISO
Lower plasma levels of G-CSF, IL-13, M-CSF, TNF-α
Higher plasma levels of GRO/KC, MCP-1, CCL3, CCL5, VEGF
@ day 7 post-injury
Lower plasma levels of G-CSF, IL-13, TNF-α
Higher plasma levels of GRO/KC, MCP-1, CCL3, CCL5, VEGF
@ day 60 post-injury
Individual NODDI variation @ day 60 post-injury
Lower NDI in ip-cor
Higher NDI in con-cor
Higher fISO
Higher plasma levels of G-CSF, IL-13, M-CSF, TNF-α
Lower plasma levels of GRO/KC, MCP-1, CCL3, CCL5, VEGF
@ day 7 post-injury
Higher plasma levels of G-CSF, IL-13, TNF-α
Lower plasma levels of GRO/KC, MCP-1, CCL3, CCL5, VEGF
@ day 60 post-injury

## Highlights

- Plasma levels of IL-1$\beta$, IL-7, CCL3, and GM-CSF were elevated from days 3 to 60 post-injury.
- Day 7 plasma marker panels were associated with trans-hemispheric cortical map transfer outcome.
- High IL-1$\beta$ and low IL-7, CCL3, and GM-CSF plasma levels at day 60 associated with worse pathology.